

Editor's Summary

Treating Cancer by Getting on Its Nerves

The nervous system plays a role in the regulation of many different organs, including the gut. Now, Zhao *et al.* have shown that the vagal nerve, which signals to the stomach through muscarinic receptors, contributes to the growth of gastric tumors. The authors demonstrated that vagotomy (surgical interruption of the vagal nerve) can prevent gastric cancer in mice and reduce the recurrence of gastric tumors in human patients. Moreover, the same result can be achieved in mice treated with Botox or anticholinergic drugs to inhibit vagal nerve signaling, raising the hope of a safer treatment for gastric cancer without irreversible side effects.

A complete electronic version of this article and other services, including high-resolution figures, can be found at:

<http://stm.sciencemag.org/content/6/250/250ra115.full.html>

Supplementary Material can be found in the online version of this article at:

<http://stm.sciencemag.org/content/suppl/2014/08/18/6.250.250ra115.DC1.html>

Information about obtaining **reprints** of this article or about obtaining **permission to reproduce this article** in whole or in part can be found at:

<http://www.sciencemag.org/about/permissions.dtl>

CANCER

Denervation suppresses gastric tumorigenesis

Chun-Mei Zhao,^{1*} Yoku Hayakawa,^{2*} Yosuke Kodama,¹ Sureshkumar Muthupalani,³ Christoph B. Westphalen,^{2,4} Gørn T. Andersen,^{1,5} Arnar Flatberg,¹ Helene Johannessen,¹ Richard A. Friedman,⁶ Bernhard W. Renz,² Arne K. Sandvik,^{1,7} Vidar Beisvag,¹ Hiroyuki Tomita,⁸ Akira Hara,⁸ Michael Quante,⁹ Zhishan Li,¹⁰ Michael D. Gershon,¹⁰ Kazuhiro Kaneko,¹¹ James G. Fox,³ Timothy C. Wang,^{2†} Duan Chen^{1†}

The nervous system plays an important role in the regulation of epithelial homeostasis and has also been postulated to play a role in tumorigenesis. We provide evidence that proper innervation is critical at all stages of gastric tumorigenesis. In three separate mouse models of gastric cancer, surgical or pharmacological denervation of the stomach (bilateral or unilateral truncal vagotomy, or local injection of botulinum toxin type A) markedly reduced tumor incidence and progression, but only in the denervated portion of the stomach. Vagotomy or botulinum toxin type A treatment also enhanced the therapeutic effects of systemic chemotherapy and prolonged survival. Denervation-induced suppression of tumorigenesis was associated with inhibition of Wnt signaling and suppression of stem cell expansion. In gastric organoid cultures, neurons stimulated growth in a Wnt-mediated fashion through cholinergic signaling. Furthermore, pharmacological inhibition or genetic knockout of the muscarinic acetylcholine M₃ receptor suppressed gastric tumorigenesis. In gastric cancer patients, tumor stage correlated with neural density and activated Wnt signaling, whereas vagotomy reduced the risk of gastric cancer. Together, our findings suggest that vagal innervation contributes to gastric tumorigenesis via M₃ receptor-mediated Wnt signaling in the stem cells, and that denervation might represent a feasible strategy for the control of gastric cancer.

INTRODUCTION

The nervous system regulates epithelial homeostasis in different ways, and this regulation by the nervous system partly involves modulation of stem and progenitor cells (1, 2). There is also crosstalk between tumor cells and nerves, such that tumors induce active neurogenesis, resulting in increased neuronal density in preneoplastic and neoplastic tissues (3–6). In addition, activation of muscarinic receptors has been shown to promote cell transformation and cancer progression (3–6). A recent study demonstrated that prostate tumors are infiltrated by autonomic nerves contributing to cancer development and dissemination (7). Given the potential ability of nerves to influence gut stem and progenitor cells, and the prevailing notion that persistently elevated gut epithelial proliferation predisposes to cancer formation, it is believed that axonal reflexes could also modulate the conversion of stem or progenitor cells into cancer cells (8, 9).

Gastric cancer is the fifth most common cancer and the third leading cause of cancer mortality worldwide, with a 5-year survival rate of less than 25% (10, 11). It has been demonstrated that vagotomy decreases

gastric mucosal thickness and cellular proliferation (12, 13). An epidemiological study showed that the risk of gastric cancer [standardized incidence ratio (SIR)] after vagotomy was not reduced during the first 10-year period, but was reduced by 50% (SIR 0.5) during the second 10-year follow-up (14, 15). Here, we provide evidence that proper innervation is critical for gastric tumorigenesis, and suggest that nerves may represent a therapeutic target for the treatment of gastric cancer.

RESULTS

Gastric lesser curvature has high vagal innervation and high incidence of tumors

In humans, there is a higher incidence of gastric cancer in the lesser (~80% of tumors) than the greater curvature (16, 17). We also observed this distribution in the INS-GAS mouse model, a genetic mouse model of spontaneous gastric cancer (18, 19), in which there was a similar prevalence (77%) of tumors in the lesser curvature (Fig. 1A). INS-GAS mice do not display obvious preneoplastic lesions until 6 months of age, but afterward, they develop gastric cancer through stages of atrophy, metaplasia, and finally, dysplasia at 12 months of age (18, 19). Topographic analysis of vagus nerve fibers and terminals in the murine stomach revealed a higher density of neurons and larger ganglia in the lesser curvature compared to the greater curvature (Fig. 1B), correlating with the observed pattern of tumor formation. This possible association between the distribution of vagal nerve fibers and the appearance of gastric tumors in INS-GAS mice prompted us to study the role of nerves in gastric tumorigenesis (fig. S1 and table S1).

Surgical denervation at preneoplastic stage attenuates tumorigenesis in mouse models of gastric cancer

In the first set of experiments, vagotomy was performed in INS-GAS mice at 6 months of age. Subsequently, the effects of vagotomy were

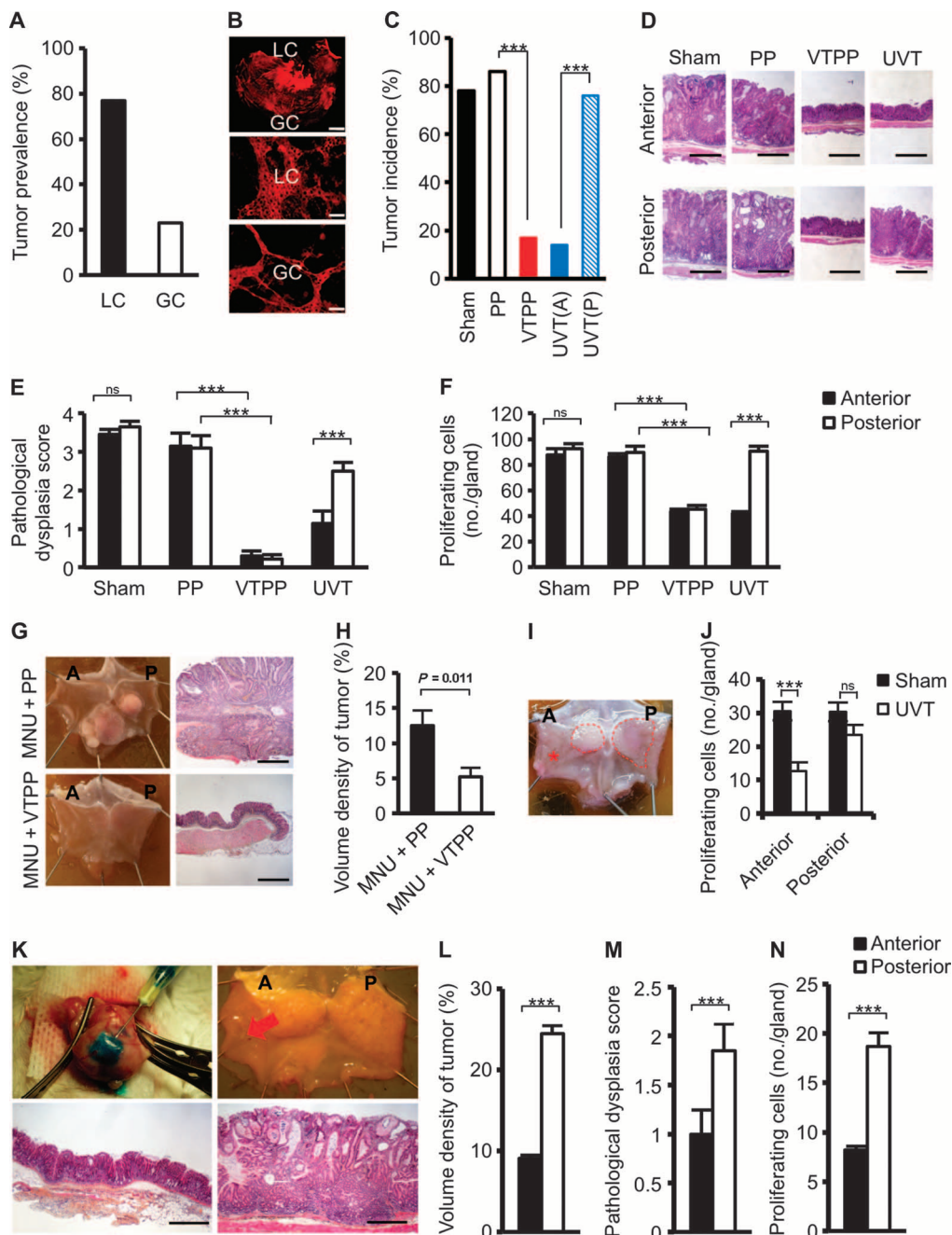
¹Department of Cancer Research and Molecular Medicine, Norwegian University of Science and Technology, Trondheim 7491, Norway. ²Division of Digestive and Liver Diseases, Columbia University College of Physicians and Surgeons, New York, NY 10032–3802, USA. ³Division of Comparative Medicine, Massachusetts Institute of Technology, Boston, MA 02139, USA. ⁴Medizinische Klinik III, Klinikum der Universität München, Campus Großhadern, 81377 München, Germany. ⁵Department of Surgery, St. Olavs University Hospital, Trondheim 7006, Norway. ⁶Biomedical Informatics Shared Resource, Herbert Irving Comprehensive Cancer Center, Columbia University College of Physicians and Surgeons, New York, NY 10032, USA. ⁷Department of Gastrointestinal and Liver Diseases, St. Olavs University Hospital, Trondheim 7006, Norway. ⁸Department of Tumor Pathology, Gifu University Graduate School of Medicine, Gifu 501-1112, Japan. ⁹Il. Medizinische Klinik, Klinikum rechts der Isar, Technische Universität München, München 81675, Germany. ¹⁰Department of Pathology and Cell Biology, Columbia University College of Physicians and Surgeons, New York, NY 10032, USA. ¹¹Department of Gastroenterology and Endoscopy Division, National Cancer Center Hospital East, Chiba 277-8577, Japan.

*These authors contributed equally to this work.

†Corresponding authors. E-mails: duan.chen@ntnu.no (D.C.); tcw21@columbia.edu (T.C.W.)

Fig. 1. Denervation attenuates tumorigenesis at the preneoplastic stage in mouse models of gastric cancer.

(A) Tumor prevalence at the lesser curvature (LC) and greater curvature (GC) of the stomach of INS-GAS mice. **(B)** Images of carbocyanine dye (DiI)-labeled vagal terminals in an adult mouse stomach. A montage of a low-power image showing the lesser curvature and greater curvature of the gastric wall (top scale bar, 2.0 mm), and higher-power images of lesser curvature (middle) and greater curvature (bottom) show a higher density of vagal innervation in lesser curvature than in greater curvature (89 and 54% of the visual field, estimated by point counting method) (middle and bottom scale bars, 72 μ m). **(C)** Tumor incidence at 12 months of age in INS-GAS mice that underwent sham operation (Sham), pyloroplasty alone (PP), bilateral vagotomy with pyloroplasty (VTPP), or anterior unilateral vagotomy (UVT) (A, anterior; P, posterior side of the stomachs) at 6 months of age. $***P = 4.9 \times 10^{-7}$ (VTPP versus PP), $P = 1.32 \times 10^{-6}$ [UVT(A) versus UVT(P)] (Fisher's exact test). **(D)** Representative microphotographs of histopathological appearance of the anterior and posterior sides of the stomach from INS-GAS mice (at 12 months of age) that underwent sham, PP, VTPP, and UVT at 6 months of age. Scale bars, 100 μ m. **(E)** Pathological score for dysplasia. Means \pm SEM. Comparisons between anterior and posterior sides were performed by paired *t* test within sham ($n = 27$) and UVT ($n = 30$), or by Tukey test between PP ($n = 25$) and VTPP ($n = 25$). $***P = 5.31 \times 10^{-5}$ (UVT), $P = 0.0001$ or 0.00006 (PP and VTPP, anterior or posterior side, respectively). ns, not significant ($P = 0.987$). **(F)** Number of proliferating cells. Means \pm SEM. Comparisons between anterior and posterior sides were performed by paired *t* test within sham ($n = 27$) and UVT ($n = 30$), or by Tukey test between PP ($n = 25$) and VTPP ($n = 25$). $***P = 5.77 \times 10^{-3}$ (UVT), $P = 1.90 \times 10^{-4}$ (anterior), and $P = 1.49 \times 10^{-3}$ (posterior) between PP and VTPP. ns, not significant ($P = 0.229$). **(G)** Representative photographs showing gross appearance of stomachs opened along the greater curvature and corresponding microphotographs of histopathological appearance of the stomachs (antrum) from mice treated with MNU + PP or MNU + VTPP. Scale bars, 100 μ m. **(H)** Volume density of tumor (measured by point counting method). Means \pm SEM. Student's *t* test was used to compare between MNU + PP ($n = 11$) and MNU + VTPP ($n = 9$). **(I)** Representative photograph showing gross appearance of gastric tumors (indicated by dashed line) in a stomach opened along the greater curvature from an *Hp*-infected H^+/K^+ -ATPase-IL-1 β mouse, which underwent UVT in the anterior side (indicated by asterisk). **(J)** Number of proliferating cells in *Hp*-infected H^+/K^+ -ATPase-IL-1 β mouse



stomachs subjected to UVT in the anterior side. Means \pm SEM. $***P = 0.00006$ (Student's *t* test). ns, not significant ($P = 0.120$) between sham ($n = 12$) and UVT ($n = 12$) in the anterior and the posterior sides. **(K)** Photographs showing the Botox injection procedure (upper left), gross appearance of Botox-injected stomach after 6 months (A, anterior where Botox was injected; P, posterior) (upper right), and representative microphotographs of histopathological appearance of anterior (lower left) and posterior (lower right) stomach (corpus). Red arrow, injection site. Scale bars, 100 μ m. **(L to N)** Volume density of tumor, pathological score for dysplasia, and number of proliferating cells after anterior Botox injection. Means \pm SEM ($n = 16$). $***P = 2.75 \times 10^{-11}$ (L), $P = 0.01$ (M), or $P = 0.001$ (N) between the anterior and posterior sides of the stomach (paired *t* test).

examined 6 months after surgery. One hundred seven INS-GAS mice were subjected to either subdiaphragmatic VTPP, UVT (fig. S2), sham operation, or PP. The unilateral vagotomy approach takes advantage of the fact that each (anterior or posterior) vagal trunk innervates only one-half of the stomach. Consequently, denervation of one side of the stomach does not impair the overall functional capacity of the stomach, leaving gastric acid output, circulating gastrin levels, and gastric motility unchanged (13, 20).

Six months after surgery, body weight was unchanged in either male or female mice (fig. S3). Tumor incidence was 17% after VTPP versus 86% after PP alone, 14% in the anterior side versus 76% in the posterior side after anterior UVT, and 78% in the sham-operated mice (Fig. 1C). Histological examination revealed the reduction of mucosal thickness after VTPP (compared to PP) or UVT (compared to the corresponding posterior side) (Fig. 1D and fig. S4), indicating successful denervation (12, 13). Pathological evaluation (21) revealed that vagotomy attenuated the score for dysplasia and reduced the number of proliferating cells (Fig. 1, E and F) and the scores for inflammation, epithelial defects, oxyntic atrophy, epithelial hyperplasia, pseudopyloric metaplasia, and gastric histological activity index (GHAI) (fig. S5, A to F).

To confirm these findings, we tested the surgical approach in two other mouse models of gastric cancer, namely, the carcinogen-induced [*N*-nitroso-*N*-methylurea (MNU)] (22) and the *Helicobacter pylori* (*Hp*)-infected H^+/K^+ -ATPase (adenosine triphosphatase)-IL-1 β (interleukin-1 β) mouse models (23). In the MNU model, VTPP performed 1 week after completion of MNU treatment inhibited tumor development at 13 months of age (Fig. 1, G and H). Infection of H^+/K^+ -ATPase-IL-1 β mice with *Hp* accelerated gastric tumorigenesis, resembling *Hp*-related atrophy-metaplasia-dysplasia sequence in humans. UVT performed 8.5 months after *Hp* infection (at 12 months of age) reduced tumor size and number of proliferating cells in the denervated side of the stomach at 18 months of age (Fig. 1, I and J). Thus, the findings from these three independent models demonstrate the importance of functional innervation in gastric tumorigenesis.

Pharmacological denervation at an early preneoplastic stage attenuates gastric tumorigenesis

To prove that the effects of surgical denervation were primarily local (acting at vagus nerve terminals within the gastric mucosa), unilateral injection of botulinum toxin A (Botox) into the gastric wall was performed in INS-GAS mice at 6 months of age. Botox enters into the axon terminal through vesicle internalization and cleaves synaptosomal-associated protein 25, leading to impaired exocytosis of neurotransmitters, including acetylcholine (24). Botox was injected subserosally along the greater curvature in the anterior side of the stomach (Fig. 1K). Six months later, tumor size, score for dysplasia, and number of proliferating cells were markedly reduced in the anterior wall compared with the posterior side of the stomach (Fig. 1, L to N). Moreover, these changes were associated with attenuated scores for inflammation, epithelial defects, atrophy, hyperplasia, pseudopyloric metaplasia, and GHAI (fig. S6, A and B). Hence, these findings confirm an important role of local signaling from vagus nerve endings in early gastric tumorigenesis.

Surgical or pharmacological denervation attenuates gastric tumor progression

Because vagotomy or Botox treatment had a protective effect at preneoplastic stages, we next examined whether gastric denervation could also inhibit tumor progression at later stages. INS-GAS mice at 8, 10,

or 12 months of age were subjected to anterior UVT and euthanized at 18 months of age. In these mice, the tumors were smaller with less severe dysplasia in the anterior side compared to the posterior side of the stomach, suggesting that denervation inhibits tumor progression in mice with established neoplastic changes (Fig. 2, A to C).

Whereas the average life span of wild-type FVB/N mice is well over 24 months, the survival of INS-GAS mice at 18 months of age was 53% (16 of 30 mice). Attenuation of tumor burden by UVT improved the 18-month survival when compared to age-matched INS-GAS mice: 71% when UVT was performed at 8 months, 64% when performed at 10 months, and 67% when performed at 12 months, respectively (Fig. 2D). Next, INS-GAS mice at 12 months of age were subjected to vehicle or Botox treatment unilaterally or bilaterally, with or without UVT. The tumor cell proliferation was reduced in the anterior side of the stomach where Botox was injected, when compared to the posterior side or vehicle-treated anterior side (Fig. 2E). The combination of UVT and Botox did not further reduce cellular proliferation, indicating that vagotomy and Botox likely act through the same mechanism. These results further suggest that surgical or pharmacological denervation inhibits gastric cancer progression even when applied at later stages of gastric tumorigenesis.

Denervation enhances the effect of chemotherapy in the treatment of gastric cancer

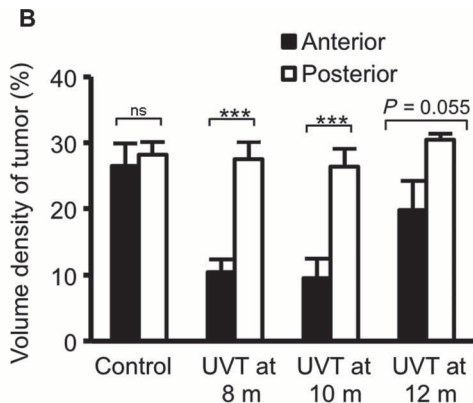
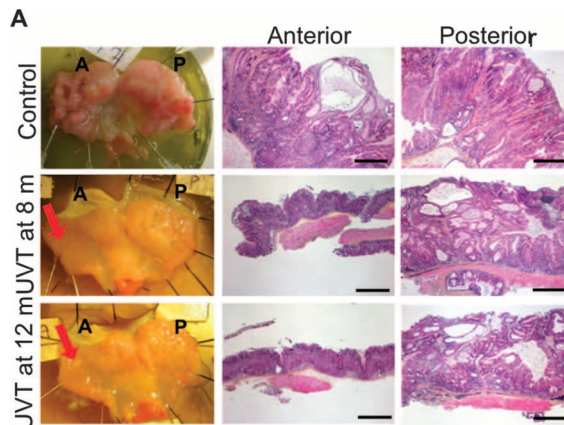
Next, we examined whether denervation could enhance the effects of systemic chemotherapy in gastric cancer. INS-GAS mice at 12 to 14 months of age received systemic administration of 5-FU + oxaliplatin or saline along with unilateral Botox treatment or UVT. The experiment was designed such that the nondenervated half of the stomach in each animal served as an internal control, either a chemotherapy-only control (the posterior side of the stomach in two of the groups received chemotherapy alone) or an untreated control. An additional group of INS-GAS mice was included as untreated controls. As early as 2 months after starting treatment, tumor size was reduced in mice treated with chemotherapy, specifically in the denervated areas of the stomach (the anterior side) after unilateral vagotomy or Botox injection (Fig. 2, F and G). The combination of either Botox or UVT with chemotherapy increased survival compared to chemotherapy alone (Fig. 2H). Together, these findings suggest that the combination of denervation and chemotherapy has an enhanced effect on tumor growth and survival.

Denervation inhibits gastric Wnt signaling and suppresses stem cell expansion through the M_3 receptor

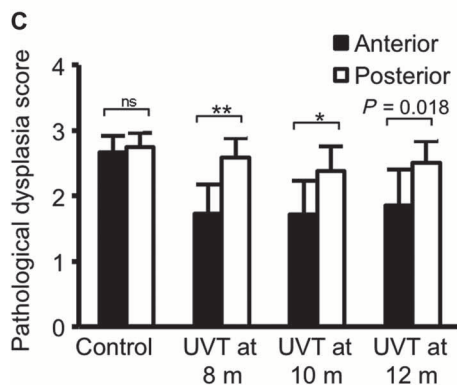
We performed gene expression profiling in INS-GAS mice versus wild-type mice, and in unilaterally vagotomized INS-GAS mice (UVT performed at 6 months of age). Comparison between INS-GAS mice and wild-type mice showed up-regulation of the Wnt signaling pathway in INS-GAS mice (fig. S7). Comparison between the vagotomized anterior and the untreated posterior side of the same stomach revealed many differentially expressed KEGG pathways, including those involved in gastric acid secretion, mitogen-activated protein kinase signaling, cell cycle, apoptosis, autophagy, vascular endothelial growth factor signaling, and actin cytoskeleton (fig. S8). The Wnt and Notch signaling pathways were markedly inhibited in the vagotomized side [validated by quantitative reverse transcription polymerase chain reaction (qRT-PCR) arrays] (Fig. 3 and fig. S9). The inhibition of Wnt signaling was persistent at 2, 6, 8, and 10 months after vagotomy.

Fig. 2. Denervation attenuates gastric tumor progression in mice.

(A) Gross appearance of mouse stomachs at 18 months of age and representative microphotographs of the histopathological appearance of the corpus region of the anterior and posterior sides of the stomach from age-matched INS-GAS mice (Control) and mice that underwent anterior UVT at 8 or 12 months of age. Scale bars, 100 μ m. Red arrows, vagotomy side.

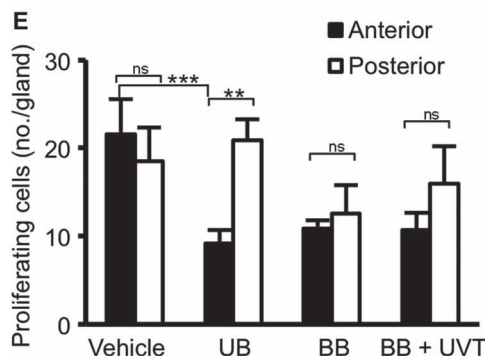


(B) Volume density of tumor. Means \pm SEM. Paired *t* test between the anterior and the posterior sides of the stomach: $P = 0.589$ ($n = 21$, Control), $P = 2.56 \times 10^{-5}$ ($n = 17$, UVT at 8 months of age), $P = 2.17 \times 10^{-4}$ ($n = 14$, UVT at 10 months), $P = 0.055$ ($n = 12$, UVT at 12 months).

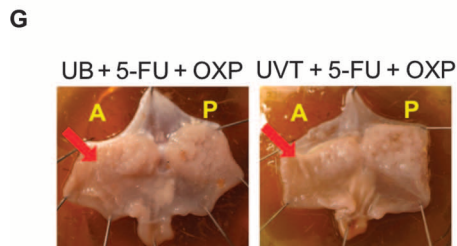


(C) Pathological score for dysplasia. Means \pm SEM. Paired *t* test between the anterior and the posterior sides of the stomach: $P = 0.38$ ($n = 21$, Control), $P = 0.002$ ($n = 17$, UVT at 8 months of age), $P = 0.047$ ($n = 14$, UVT at 10 months), $P = 0.018$ ($n = 12$, UVT at 12 months).

(D) Kaplan-Meier curves showing survival of INS-GAS mice that underwent UVT at 8 (red), 10 (green), or 12 months of age (blue), or of age-matched INS-GAS mice (Control) (black).

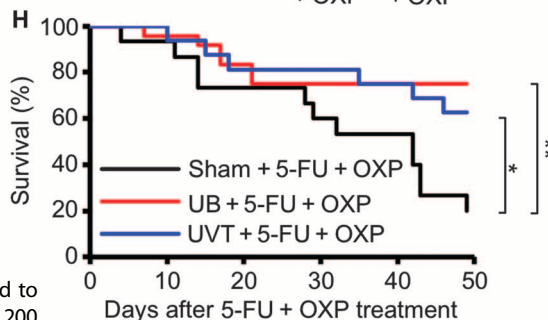
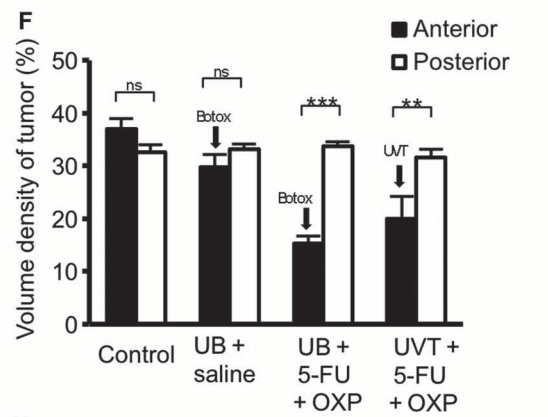
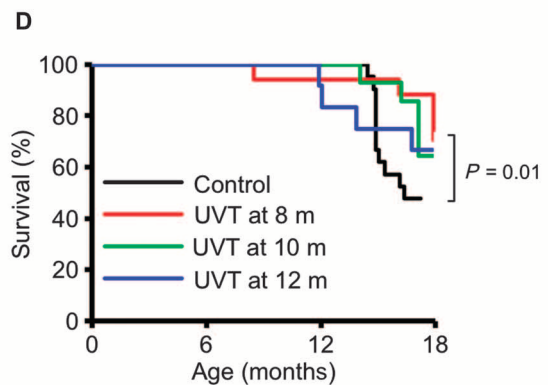
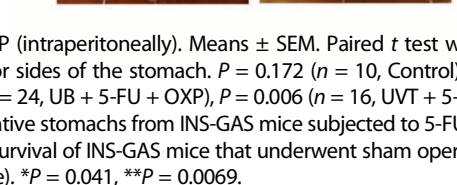


$P = 0.01$ between control and UVT groups at 8 months. **(E)** Proliferating cells in the anterior and posterior mucosa of the stomach of INS-GAS mice at 2 months after vagotomy and/or Botox injection. Means \pm SEM. Paired *t* test was used to compare the anterior and posterior sides of the stomach. $P = 0.291$ ($n = 6$, Vehicle), $P = 0.007$ [$n = 6$, unilateral anterior Botox (UB)], $P = 0.595$ [$n = 7$, bilateral Botox (BB)], $P = 0.326$ [$n = 7$, bilateral Botox plus anterior UVT (BB + UVT)], $P = 0.0007$ (Vehicle anterior versus UB anterior, Dunnett's test).



(F) Volume density of tumor in INS-GAS mice subjected to saline (intraperitoneally) (Control), UB + saline (intraperitoneally), UB + 5-fluorouracil (5-FU) + oxaliplatin (OXP) (intraperitoneally), or UVT + 5-FU + OXP (intraperitoneally). Means \pm SEM. Paired *t* test was used to compare the anterior and posterior sides of the stomach. $P = 0.172$ ($n = 10$, Control), $P = 0.200$ ($n = 10$, UB + saline), $P = 0.0004$ ($n = 24$, UB + 5-FU + OXP), $P = 0.006$ ($n = 16$, UVT + 5-FU + OXP).

(G) Gross appearance of representative stomachs from INS-GAS mice subjected to 5-FU + OXP with UB or UVT (reduced tumor burden indicated by arrows). **(H)** Kaplan-Meier curves showing survival of INS-GAS mice that underwent sham operation and 5-FU + OXP treatment (black), UB and 5-FU + OXP (red), or anterior UVT and 5-FU + OXP (blue). * $P = 0.041$, ** $P = 0.0069$.



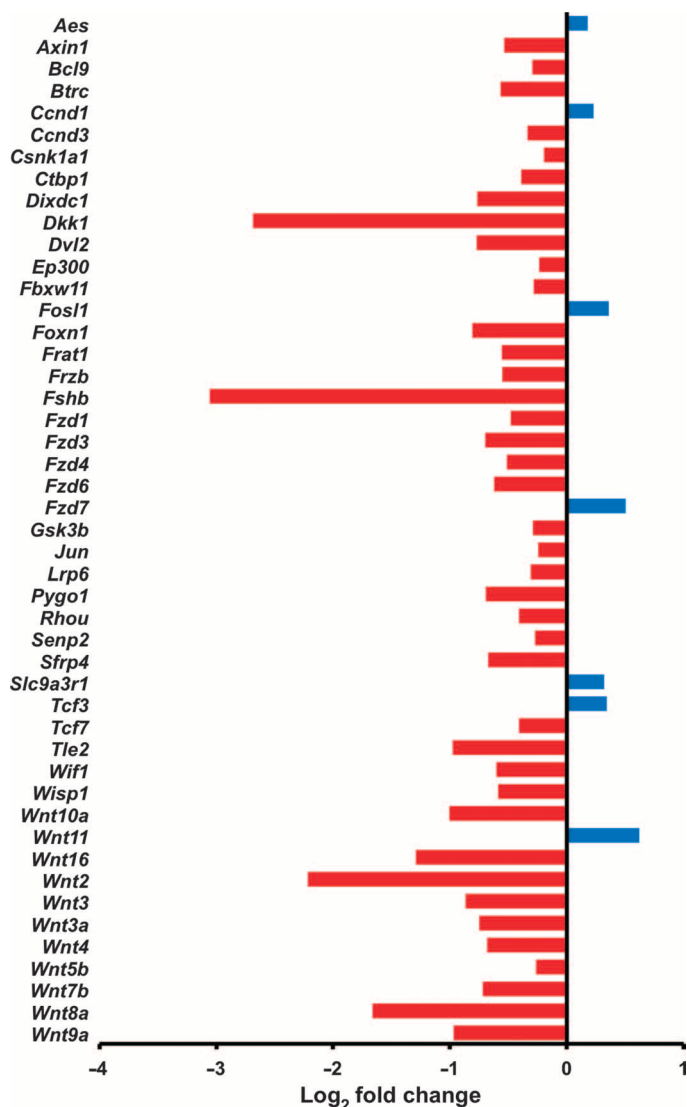


Fig. 3. Denervation leads to inhibition of Wnt signaling in the mouse model of gastric cancer. Gene expression of Wnt signaling pathway (determined by qRT-PCR array analysis) in vagotomized anterior stomach of INS-GAS mice at 12 months of age (6 months UVT). Log₂ fold changes of expressed genes in comparison with the posterior side of the same stomach are shown. Red, down-regulation; blue, up-regulation.

Inflammation-related pathways, including T cell receptor signaling, natural killer cell-mediated cytotoxicity, leukocyte transendothelial migration, and chemokine signaling, were activated at 2 months, but then inhibited at 4 and 6 months after vagotomy, whereas Toll-like receptor signaling was inhibited at all the time points (Fig. 4A).

The Wnt signaling pathway is a major regulator of gastrointestinal stem cells and tumorigenesis (25, 26). CD44 is a known target of the Wnt signaling pathway (27) and has been shown to label a cancer-initiating cell population (28). *Lgr5* is a marker of gastric stem cells in normal as well as cancer tissues, and also a target of the Wnt signaling pathway (29). Either vagotomy (VTPP and UVT) or Botox treatment induced down-regulation of CD44 (and CD44v6) in the gastric mucosa of INS-GAS mice, although the combination of vagotomy and

Botox did not lead to a further decrease in CD44 expression (Fig. 4, B and C, and figs. S10 and S11). Vagotomy also reduced the expression of Wnt target genes, such as *Cyclin D1*, *Axin2*, *Myc*, *Lgr5*, and *Cd44*, in MNU-treated mice (Fig. 4D). The number of cells with nuclear translocation of β -catenin and the number of *Lgr5*⁺ cells in MNU-treated mice were reduced after vagotomy (Fig. 4, E and F). These results suggest that disruption of neuronal signaling inhibits Wnt signaling and thereby stem cell expansion, resulting in the suppression of tumor development in both INS-GAS and MNU mouse models.

Wnt signaling is also known to be involved in tumor regeneration (30). We have established a mouse model of tumor regeneration through topical application of acetic acid in INS-GAS mice (31). In this model, vagotomy delayed tumor regeneration in the denervated side of the stomach (fig. S12).

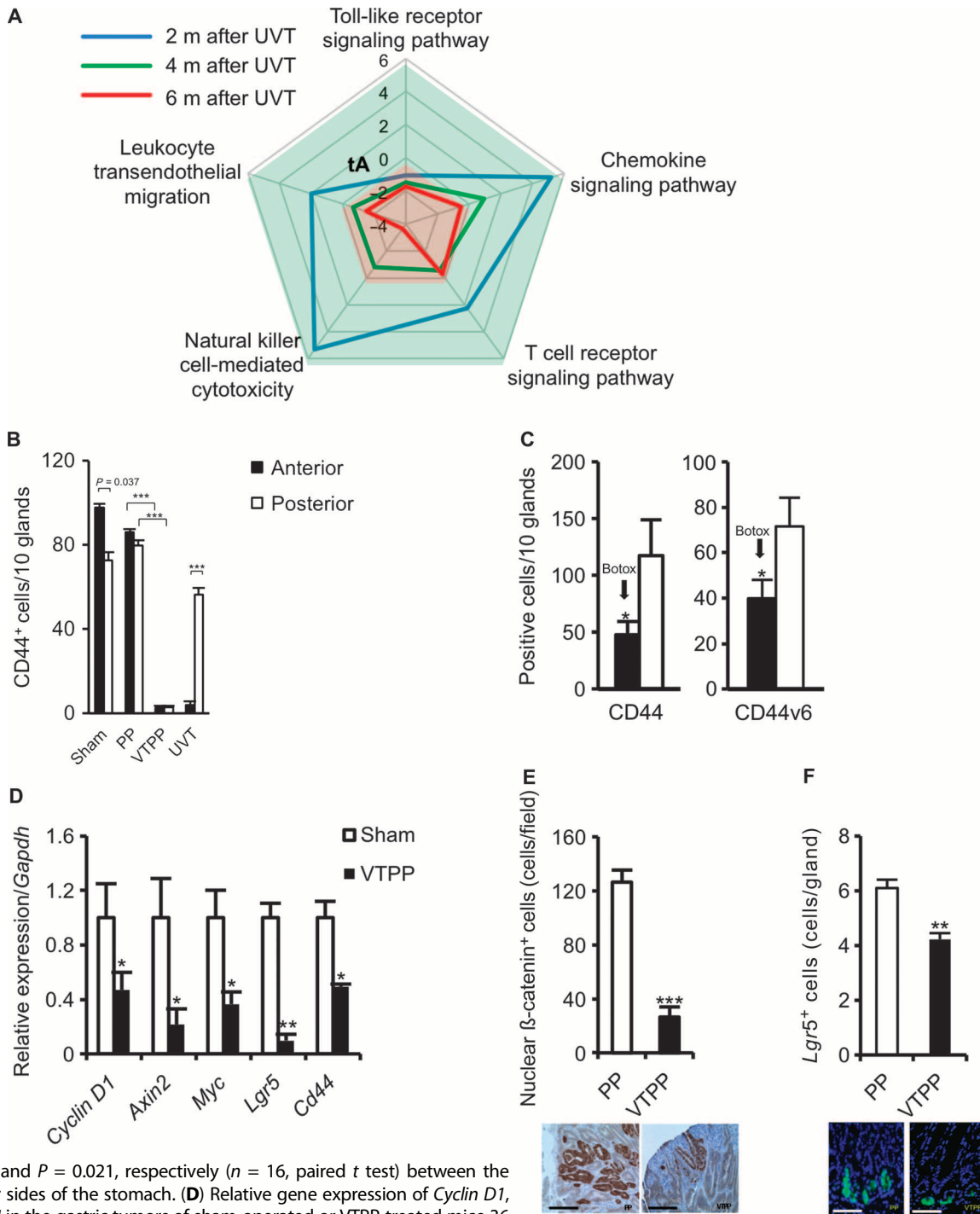
We next examined whether vagotomy down-regulated *Lgr5* expression via the muscarinic acetylcholine receptors. Gastric epithelial cells from *Lgr5*-GFP mice were sorted on the basis of green fluorescent protein (GFP) expression. Afterward, gene expression of the muscarinic acetylcholine receptors was tested in *Lgr5*-negative, *Lgr5*-low, and *Lgr5*-high cell populations (Fig. 5A). We found that there was coexpression of *Lgr5* and *Chrm3*, the gene encoding muscarinic acetylcholine receptor 3 (M₃R), in the sorted cells from *Lgr5*-GFP mouse stomach, but other subtypes of muscarinic receptor were little expressed in those cells (Fig. 5, B and C), suggesting that *Lgr5*⁺ stem cell function may be modulated by M₃R signaling. To investigate the involvement of M₃ receptors in gastric tumorigenesis, we treated INS-GAS mice by continuous infusion of the specific M₃ receptor antagonist, darifenacin (32), in combination with chemotherapy. Using an experimental design similar to that of the Botox and vagotomy experiment, we found that the combination of darifenacin and chemotherapy reduced cellular proliferation of the tumors (Fig. 5D). Furthermore, we analyzed the Wnt signaling pathway in M₃KO versus wild-type mice and found that several key genes, including one encoding β -catenin, were down-regulated (fig. S13). We then exposed M₃KO and wild-type mice to MNU treatment. At 7.5 months after MNU treatment (11 months of age), M₃KO mice had less tumor induction (57.1% versus 100%) and smaller tumor size when compared to wild-type controls (Fig. 5, E and F). Thus, the vagus nerve regulates gastric tumorigenesis at least in part through M₃ receptor-mediated Wnt signaling, which is operative in *Lgr5*⁺ stem cells.

Neurons activate Wnt signaling in gastric stem cells through M₃ receptor

To demonstrate the potential regulatory role of nerves in the maintenance of gastric epithelium, we used an established in vitro culture system for gastric organoids (9). Primary neurons were isolated from murine spinal cord or the enteric nervous system of guinea pigs, and cocultured with gastric glands (9, 33, 34). In culture, neurons showed outgrowth of neurites and evidence of direct contact with the gastric organoids (Fig. 6, A to C). Furthermore, coculture with neurons markedly promoted gastric organoid growth (Fig. 6, D and E). The addition of either Botox or scopolamine (an unspecific muscarinic receptor antagonist) inhibited this stimulatory effect (Fig. 6, D and E), whereas pilocarpine (an unspecific muscarinic receptor agonist) stimulated organoid growth (Fig. 6F). Pilocarpine caused up-regulation of the gastric stem cell markers and Wnt target genes *Lgr5*, *Cd44*, and *Sox9* (9) in a dose-dependent manner. However, in gastric organoids of M₃KO mice,

Fig. 4. Denervation alters inflammation-related signaling and suppresses stem cell expansion in mouse models of gastric cancer.

(A) Time course of five signaling pathways determined by microarray analysis in the anterior side of the stomach at 2 (blue), 4 (green), and 6 (red) months after anterior UVT compared with the posterior side of the stomach in INS-GAS mice. Total net accumulated perturbation (expressed as tA score): -4 to 6. tA score > 0: activation; tA score < 0: inhibition. **(B)** Numbers of CD44⁺ cells in the anterior and the posterior sides of the stomach of INS-GAS mice at 6 months after surgery. Means ± SEM. $P = 0.037$ ($n = 27$, paired t test) between the anterior and the posterior sides in sham operation (Sham), $P = 1.00 \times 10^{-6}$ or $P = 6.00 \times 10^{-6}$ ($n = 25$, Dunnett's test) between PP and VTPP (anterior and posterior sides, respectively), and $P = 1.74 \times 10^{-3}$ ($n = 30$, paired t test) between the anterior and the posterior sides within anterior UVT. **(C)** Numbers of CD44-immunoreactive cells (CD44) and CD44v6-immunoreactive cells (CD44v6) in the anterior and the posterior sides of the stomach of INS-GAS mice at 6 months after Botox injection. Means ± SEM. $P = 0.034$ and $P = 0.021$, respectively ($n = 16$, paired t test) between the anterior and the posterior sides of the stomach. **(D)** Relative gene expression of *Cyclin D1*, *Axin2*, *Myc*, *Lgr5*, and *Cd44* in the gastric tumors of sham-operated or VTPP-treated mice 36 weeks after MNU treatment ($n = 4$ per group). Means ± SEM. $P = 0.04$ (*Cyclin D1*), 0.04 (*Axin2*), 0.03 (*Myc*), 0.001 (*Lgr5*), and 0.01 (*Cd44*) (Student's t test). **(E)** Number of cells showing nuclear β-catenin accumulation in the gastric tumors of PP- or VTPP-treated mice 36 weeks after MNU treatment ($n = 4$ per group). Means ± SEM. $P = 7.00 \times 10^{-6}$ (Student's t test). Representative immunohistochemical microphotographs are shown below. Scale bars, 40 μm. **(F)** Number of *Lgr5*⁺ cells in the stomachs of PP- or VTPP-treated mice 6 weeks after MNU treatment ($n = 5$ per group). Means ± SEM. $P = 4.00 \times 10^{-6}$ (Student's t test). Representative *Lgr5*-GFP⁺ microphotographs are shown below. Scale bars, 20 μm.



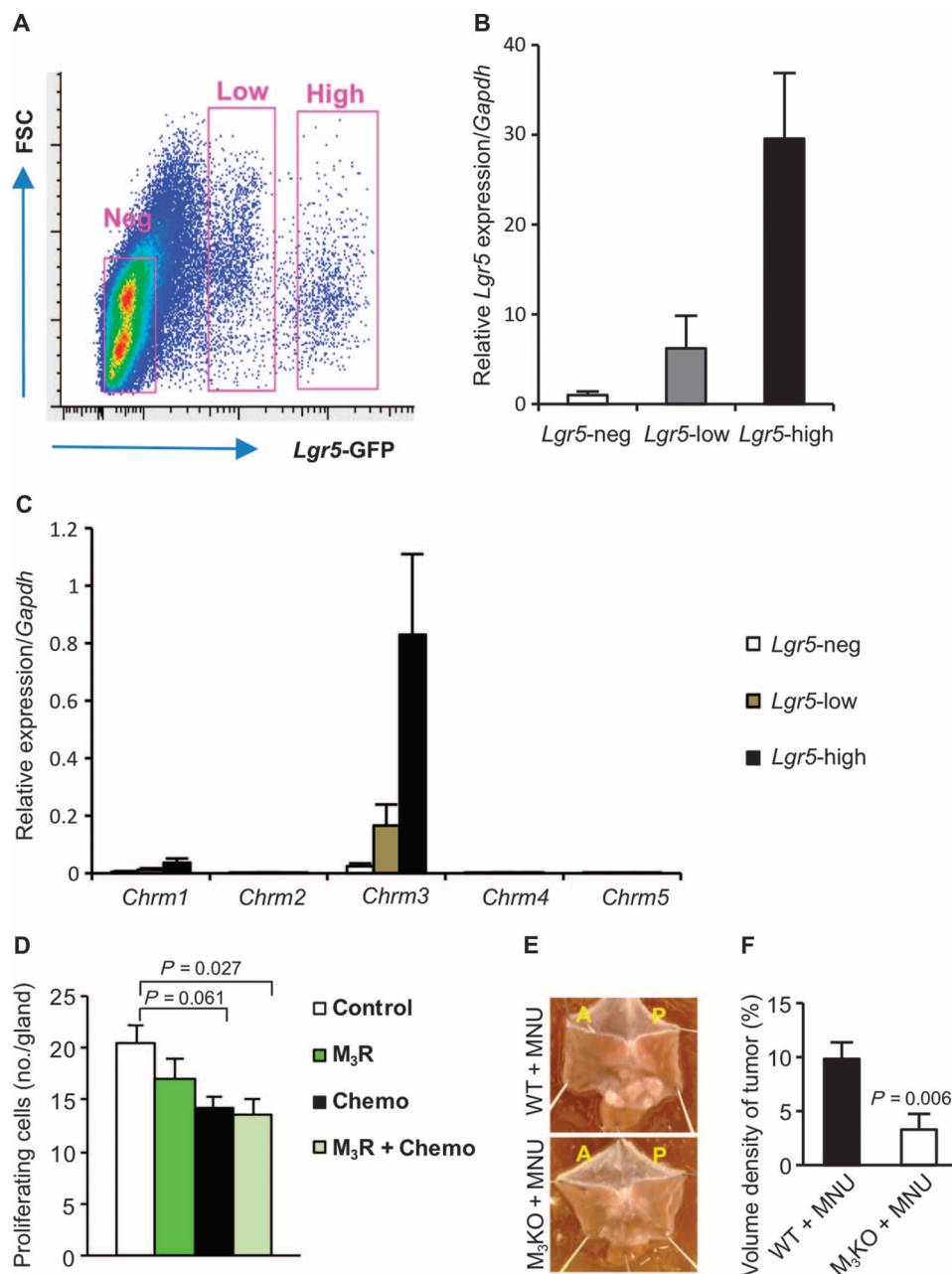


Fig. 5. M_3 receptor signaling in gastric stem cells regulates tumorigenesis in mouse models of gastric cancer. (A) Representative fluorescence-activated cell sorting gating showing forward scatter (FSC) and *Lgr5*-GFP expression. (B and C) Relative gene expression of *Lgr5* and muscarinic receptors (*Chrm1* to *Chrm5*) in sorted *Lgr5*-negative, *Lgr5*-low, and *Lgr5*-high populations. Means \pm SEM ($n = 4$). (D) Number of proliferating cells in the tumors of INS-GAS mice treated with saline (Control, $n = 19$), M_3 receptor antagonist darifenacin (M_3R , $n = 15$), 5-FU + oxaliplatin (Chemo, $n = 12$), or combination of 5-FU + oxaliplatin + darifenacin (M_3R + Chemo, $n = 8$), respectively. Means \pm SEM. P values were calculated by Dunnett's test. (E) Representative photographs showing gross appearance of stomachs opened along the greater curvature from wild-type (WT) or M_3 receptor knockout mice (M_3KO) treated with MNU. (F) Volume density of tumor in the stomachs of MNU-treated WT ($n = 13$) versus MNU-treated M_3KO mice ($n = 7$). Means \pm SEM (Student's t test).

pilocarpine showed no effects on the expression of these genes (Fig. 6G), highlighting the importance of the M_3 receptor for stem cell expansion. Furthermore, coculture with neurons could substitute for Wnt3a

in gastric organoid cultures that are otherwise strictly dependent on addition of Wnt ligands (35) (Fig. 6H), confirming the ability of cholinergic signaling to induce ligand-independent Wnt signaling in this in vitro system.

Gastric cancer patients display dysregulation of Wnt signaling and innervation in the tumors

To further investigate the involvement of Wnt signaling, innervation, and gastric cancer progression in humans, we evaluated three separate cohort studies of gastric cancer patients (table S2). In tumors from 17 primary gastric cancer patients, Wnt signaling, neurotrophin signaling, and axonal guidance pathways (along with other pathways) were activated in cancerous tissue when compared to adjacent noncancerous tissue (Fig. 7 and fig. S14). In another group of 120 primary gastric cancers, neuronal density was correlated with more advanced tumor stages (Fig. 8, A to C). A similar increase in neuronal density was confirmed in tumors of mice treated with MNU (Fig. 8, D to F). In the third cohort of 37 patients, who developed gastric stump cancer after distal gastrectomy with or without vagotomy, 35% (13 of 37) of patients had undergone vagotomy. Of those 13 patients, only 1 had a tumor in the posterior wall and none had tumors in the anterior wall. In the 24 patients without vagotomy, tumors were observed in both anterior and posterior walls (fig. S15).

DISCUSSION

The results of the present study, using three independent mouse models of gastric cancer, demonstrate that either surgical or pharmacological denervation suppresses gastric tumorigenesis. The effect takes place primarily on terminal and intramucosal vagal branches, as shown by the response to unilateral vagotomy and localized Botox injection. Denervation therapy was effective in both early preneoplasia and late neoplasia/dysplasia, and it enhanced the effect of chemotherapy and prolonged survival in mice with advanced tumors. Gene expression and immunohistochemical analysis of stem cell markers,

along with the in vitro gastric organoid test, revealed that cholinergic nerves directly modulate epithelial stem cells through activation of Wnt signaling via the M_3 receptor. Analysis of human patients with

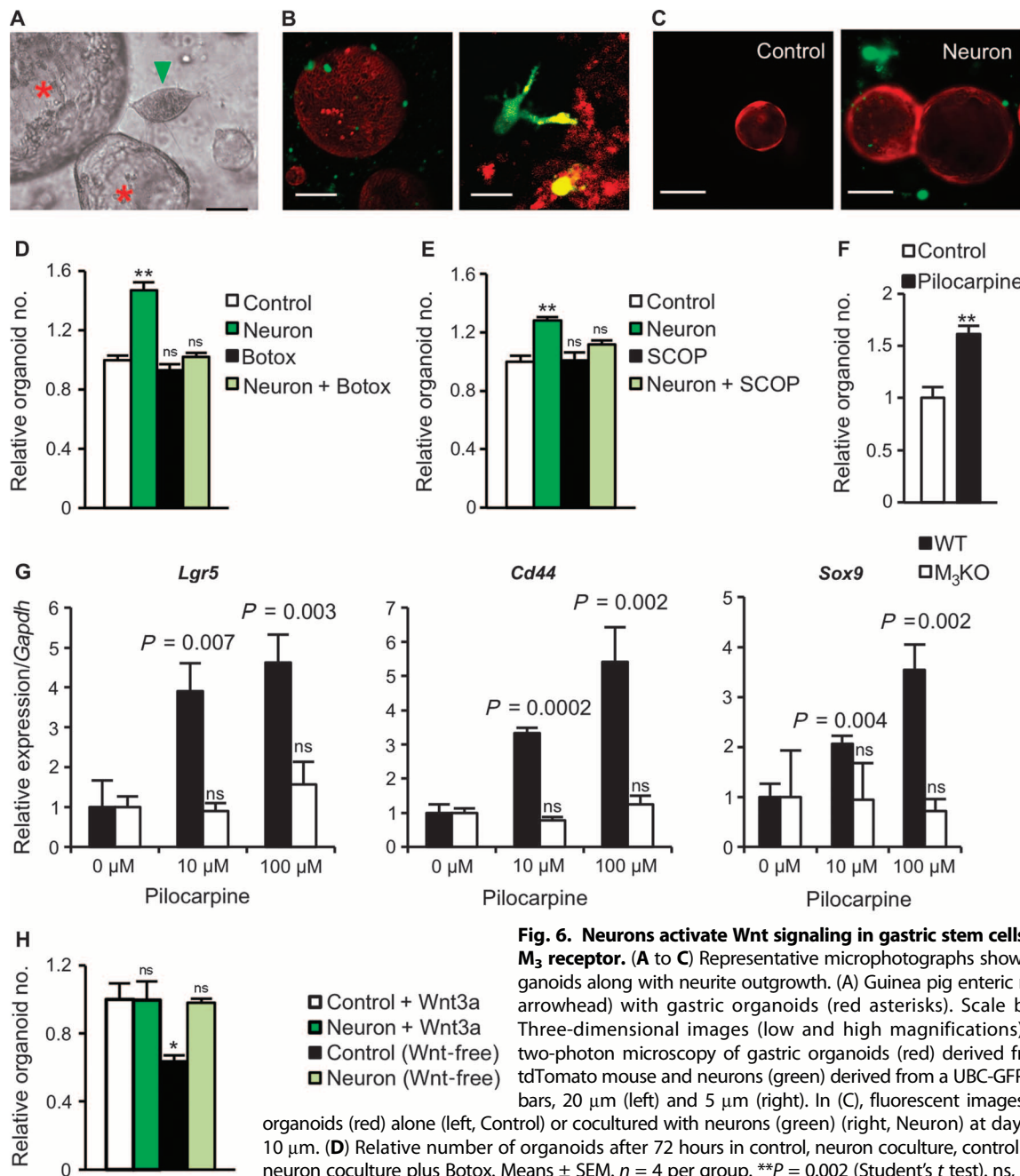


Fig. 6. Neurons activate Wnt signaling in gastric stem cells through the M₃ receptor.

(A to C) Representative microphotographs showing gastric organoids along with neurite outgrowth. (A) Guinea pig enteric neuron (green arrowhead) with gastric organoids (red asterisks). Scale bar, 5 μm. (B) Three-dimensional images (low and high magnifications) obtained by two-photon microscopy of gastric organoids (red) derived from an ACTB-tdTomato mouse and neurons (green) derived from a UBC-GFP mouse. Scale bars, 20 μm (left) and 5 μm (right). In (C), fluorescent images show gastric organoids (red) alone (left, Control) or cocultured with neurons (green) (right, Neuron) at day 4. Scale bars, 10 μm. (D) Relative number of organoids after 72 hours in control, neuron coculture, control plus Botox, or neuron coculture plus Botox. Means ± SEM. $n = 4$ per group. $**P = 0.002$ (Student's t test). ns, not significant compared to control. (E) Relative number of organoids after 72 hours in control or neuron coculture with or

without scopolamine (SCOP) (1 μg/ml). Means ± SEM. $n = 4$ per group. $**P = 0.003$ (Student's t test). ns, not significant compared to control. (F) Relative number of organoids at day 10 with or without 100 μM pilocarpine. Means ± SEM. $n = 4$ per group. $**P = 0.006$ (Student's t test) between control and pilocarpine. (G) Relative mRNA expression for *Lgr5*, *Cd44*, and *Sox9* in relation to *Gapdh* on day 7 with or without 10 or 100 μM pilocarpine in gastric organoids isolated from WT or M₃KO mice. Means ± SEM. Student's t test between 0 μM and 10 or 100 μM pilocarpine. $n = 4$ per group. (H) Relative number of organoids at day 10 with or without neurons and/or Wnt3a. Means ± SEM. $n = 4$ per group. ns, not significant. $*P = 0.030$ compared to Control + Wnt3a (Student's t test).

gastric cancer also showed correlations between neural pathways and Wnt signaling and increased innervation in more advanced tumors, with decreased tumor risk in vagotomized stomach.

In contrast to our current results, previous vagotomy studies in rat models of chemically induced gastric cancer did not reveal an inhibitory effect (12, 36, 37). This is likely due to the earlier approach of

bilateral vagotomy without pyloroplasty, which delayed gastric emptying and therefore increased the exposure time of orally administered chemical carcinogens on the gastric mucosa. To ensure that dose and time of MNU exposure were equalized in all the groups and to prevent retention of gastric contents, we performed bilateral vagotomy with pyloroplasty or PP (as control) after completion of the MNU dosing

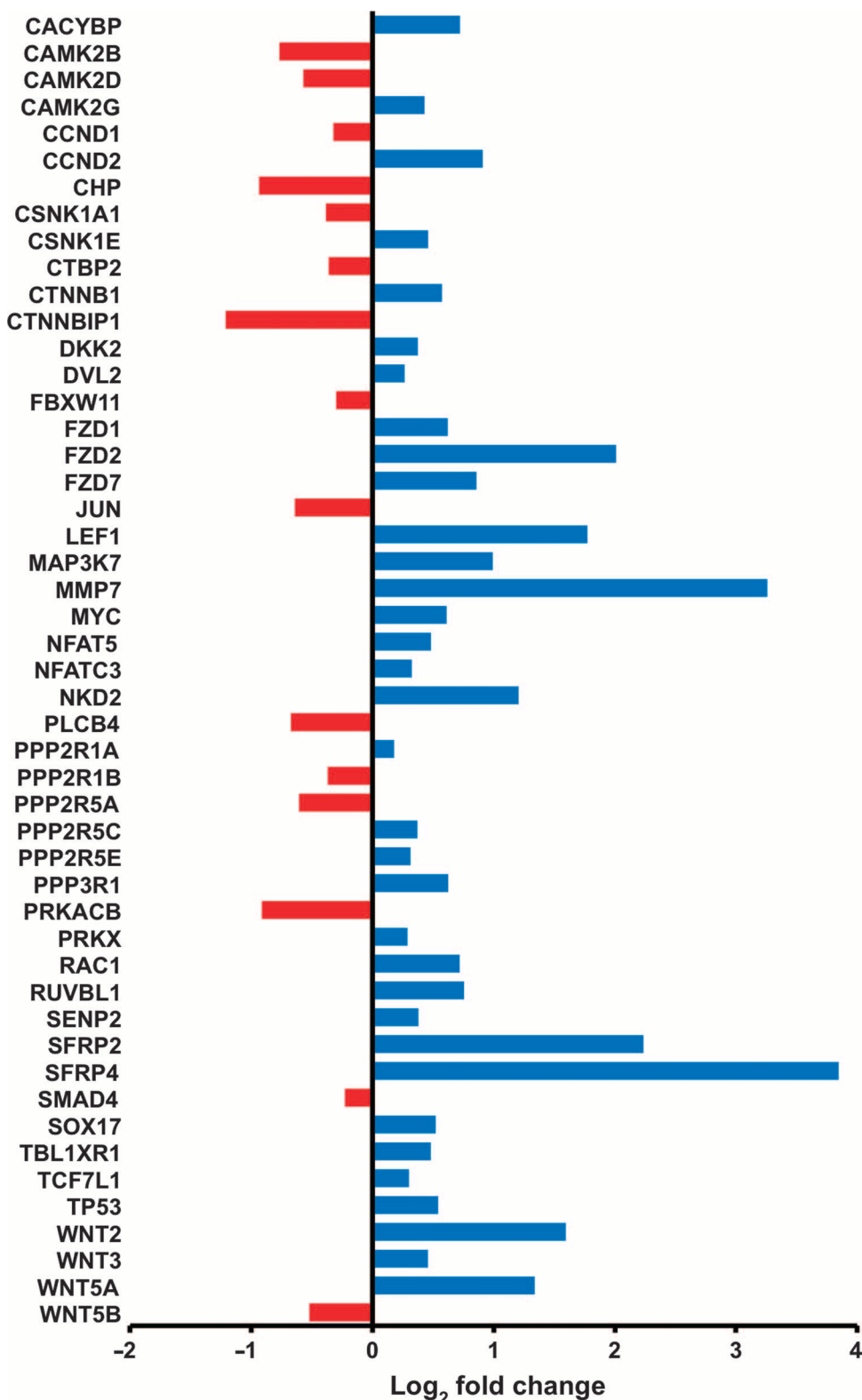


Fig. 7. Gastric cancer patients exhibit a dysregulation of Wnt signaling. Gene expression of Wnt signaling pathway (microarray analysis) in human gastric cancer tissue. The graph shows log₂ fold changes of expressed genes in comparison with the adjacent noncancerous tissue of the same stomach. Red, down-regulation; blue, up-regulation.

protocol, allowing analysis of the specific effects of the vagus nerve on the gastric mucosa. Thus, we found that vagotomy inhibited gastric tumorigenesis in the MNU model. The data from two different genetically engineered mouse models of gastric cancer further established the inhibitory effect of denervation against gastric tumorigenesis. Given the limited availability of metastatic models of gastric cancer, the effect of denervation in metastatic lymph nodes or other organs remains unclear and needs to be further investigated in suitable models.

Previous studies suggested that nerves contribute to the normal stem cell niche (1, 2, 38), and a recent report has linked sympathetic nerves to prostate cancer progression (7). However, the stomach differs from other solid organs in that its autonomic innervation is largely parasympathetic in nature, and cholinergic nerves have been shown to regulate gastrointestinal proliferation (39). The present study demonstrated that *Lgr5*⁺ gastric stem cells express the M₃ receptor, and that Wnt signaling in those cells is directly activated by cholinergic vagus stimulation, resulting in epithelial proliferation and stem cell expansion. Gastrointestinal stem cells are supported by a number of niche cells including Paneth cells, mesenchymal stem cells, myofibroblasts, smooth muscle cells, lymph and vascular endothelial cells, and bone marrow-derived stromal cells (40–42). Here, we identified nerves regulating gastric stem cell expansion during the tumorigenesis.

The vagus nerve has been shown to stimulate cell proliferation in the brain, liver, and stomach through the M₃ receptor (43–45). Furthermore, activation of muscarinic receptors in cancer cells leads to enhanced Wnt signaling independent of Wnt ligands (46), and M₃ receptor signaling has been implicated in the pathogenesis of intestinal neoplasia (6, 47, 48). Consistent with those findings, the present study demonstrates that genetic knockout or pharmacological inhibition of M₃ receptor suppresses gastric tumor progression, pointing to the M₃ receptor as a potential target for gastric cancer therapy. The M₃ receptor antagonist darifenacin is already in clinical use for overactive urinary bladder (49) and has been shown to inhibit growth of small cell lung cancer xenografts (50). Given

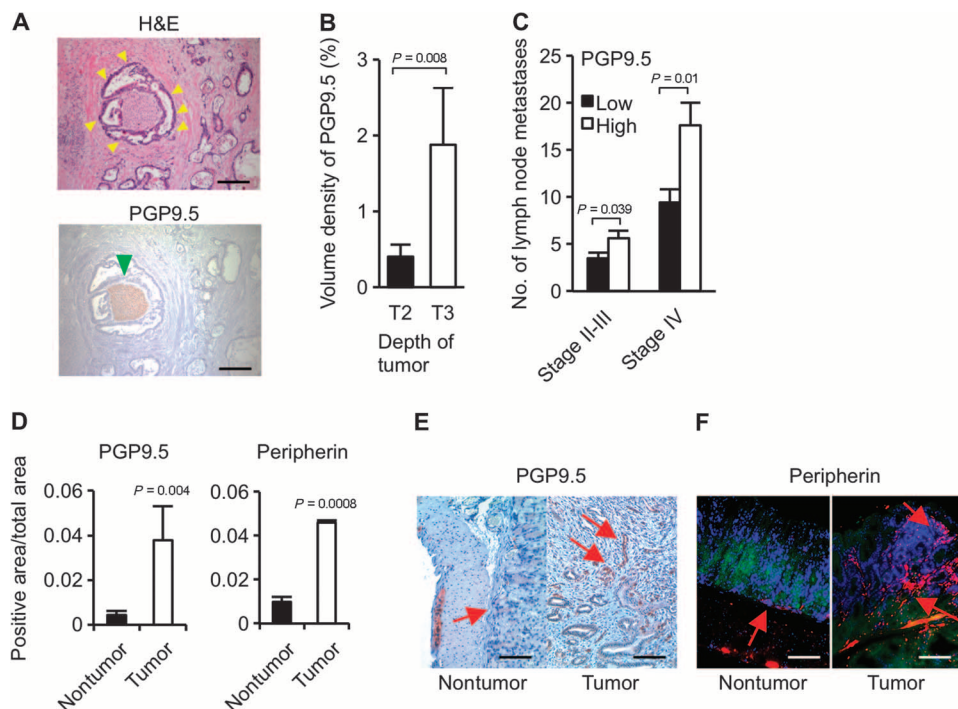


Fig. 8. PGP9.5 and peripherin may represent neural markers for gastric cancer progression. (A) Representative microphotographs showing human gastric cancer [indicated by yellow arrowheads, hematoxylin and eosin (H&E) staining] and PGP9.5-labeled nerve (green arrowhead). Scale bars, 50 μ m. (B) Volume density of PGP9.5-labeled nerves in different levels of depth of tumor invasion [T2 (tumor invading muscularis propria) versus T3 (tumor penetrating subserosal connective tissue without invasion of visceral peritoneum or adjacent structures)] in the stage II and III gastric cancer patients. Means \pm SEM ($n = 120$). $P = 0.008$ (Student's t test). (C) Number of lymph node metastases in patients with stage II and III or stage IV gastric cancer that has low or high expression of PGP9.5. Means \pm SEM ($n = 120$). P values were calculated by Student's t test. (D) PGP9.5- and peripherin-immunoreactive nerve densities in gastric mucosa of control mice (nontumor) and MNU-treated mice (tumor). PGP9.5 is a ubiquitin-protein hydrolase that is expressed in the neuronal cell bodies and axons in the central and peripheral nervous system. Peripherin is a type III intermediate filament protein that is expressed in peripheral and some central nervous system neurons. Both can be used as neuronal markers in the gut. Means \pm SEM ($n = 6$ per group). P values were calculated by Student's t test. (E and F) Representative immunohistochemical microphotographs showing PGP9.5 and peripherin (indicated by red arrows) in the nontumor and tumor areas of the mouse stomachs. Scale bars, 20 μ m (E) and 40 μ m (F).

that chemotherapeutic agents and darifenacin appear to show cooperative effects, M_3 receptor-targeting therapy combined with chemotherapy in unresectable gastric cancer patients could be considered in future trials, although further studies are needed to evaluate the safety and long-term effects of those regimens.

Canonical Wnt signaling controls epithelial homeostasis in the intestine and the stomach, and is thought to play a role in a subset of gastric cancers (9, 51). Here, we have shown that Wnt signaling is up-regulated in the tumorigenic stomach and is down-regulated after vagotomy, suggesting that vagus nerve is a critical regulator of Wnt signaling in gastric tumorigenesis. Furthermore, gastric Wnt signaling was down-regulated in M_3 KO mice, which were resistant to MNU-induced tumorigenesis. In addition, inhibition of Notch signaling was also observed after vagotomy, which is in line with both Wnt and Notch signaling promoting the initiation of intestinal tumors (52, 53). Therefore, therapeutic modulation of Wnt signaling blockade using tankyrase inhibitors could also be considered, although the dose-limiting toxicity

of available agents has restricted their clinical use to this point (54). Finally, we cannot exclude a role for additional pathways (for example, prostaglandin E_2 pathway) that may be modulated by nerves in gastric tumorigenesis.

Our finding that nerves play an important role in cancer initiation and progression highlights a component of the tumor microenvironment contributing to the cancer stem cell niche. The data strongly support the notion that denervation and cholinergic antagonism, in combination with other therapies, could represent a viable approach for the treatment of gastric cancer and possibly other solid malignancies.

MATERIALS AND METHODS

We used 581 mice divided into 14 experimental groups. In each experiment, mice were randomly divided into different subgroups (fig. S1 and table S1). INS-GAS mice with spontaneous gastric cancer were used as previously described (18, 19). Denervation was achieved by subdiaphragmatic bilateral truncal vagotomy, unilateral vagotomy, or Botox local injection. The tumor prevalence/incidence, tumor size, tumor regeneration, pathological changes, gene expression profiles, and immunohistochemical biomarkers were examined after denervation. In vitro gastric organoid culture was performed as described previously (9). We also performed three cohort studies of human primary gastric cancer and gastric stump cancer, as well as gene expression profiling and KEGG pathway analysis. All studies and procedures involving animals and human subjects were approved by the Norwegian National Animal Research Authority, the Columbia University Institutional Animal Care and Use Committee, Gifu University, and the National Cancer Center Hospital East, Japan. Statistical comparisons were performed between experimental groups, between the anterior and posterior sides of the stomachs, and between groups of patients. See the Supplementary Materials for the complete Materials and Methods.

human subjects were approved by the Norwegian National Animal Research Authority, the Columbia University Institutional Animal Care and Use Committee, Gifu University, and the National Cancer Center Hospital East, Japan. Statistical comparisons were performed between experimental groups, between the anterior and posterior sides of the stomachs, and between groups of patients. See the Supplementary Materials for the complete Materials and Methods.

SUPPLEMENTARY MATERIALS

www.sciencetranslationalmedicine.org/cgi/content/full/6/250/250ra115/DC1
Materials and Methods

Fig. S1. Flowchart showing the animal study design.

Fig. S2. Anterior UVT in mice.

Fig. S3. Body weight of male and female INS-GAS mice after surgery.

Fig. S4. Thickness of the gastric oxyntic mucosa after surgery in INS-GAS mice.

Fig. S5. Pathological scores for the stomach after surgery in INS-GAS mice.

Fig. S6. Pathological scores for the stomach after Botox injection in INS-GAS mice.
 Fig. S7. Wnt signaling in INS-GAS mice compared with wild-type mice.
 Fig. S8. Altered signaling pathways after vagotomy in INS-GAS mice.
 Fig. S9. Wnt and Notch signaling pathways after vagotomy in INS-GAS mice.
 Fig. S10. Immunostaining of CD44 after vagotomy in INS-GAS mice.
 Fig. S11. Numbers of CD44-immunoreactive cells after Botox treatment \pm vagotomy in INS-GAS mice.
 Fig. S12. Tumor regeneration in the stomach after vagotomy in INS-GAS mice.
 Fig. S13. Wnt signaling KEGG pathway in M₃KO mice compared with wild-type mice.
 Fig. S14. Altered signaling pathways in human gastric cancer tissue compared with adjacent noncancerous tissue.
 Fig. S15. Gastric stump cancer after distal gastrectomy with or without vagotomy.
 Fig. S16. Effect of 5-FU and oxaliplatin in INS-GAS mice.
 Table S1. Animal experimental groups.
 Table S2. Cohorts of gastric cancer patients.
 Table S3. List of qRT-PCR primers used in this study.

REFERENCES AND NOTES

- Y. Katayama, M. Battista, W. M. Kao, A. Hidalgo, A. J. Peired, S. A. Thomas, P. S. Frenette, Signals from the sympathetic nervous system regulate hematopoietic stem cell egress from bone marrow. *Cell* **124**, 407–421 (2006).
- O. Lundgren, M. Jodal, M. Jansson, A. T. Ryberg, L. Svensson, Intestinal epithelial stem/progenitor cells are controlled by mucosal afferent nerves. *PLoS One* **6**, e16295 (2011).
- R. R. Mattingly, A. Sorisky, M. R. Brann, I. G. Macara, Muscarinic receptors transform NIH 3T3 cells through a Ras-dependent signalling pathway inhibited by the Ras-GTPase-activating protein SH3 domain. *Mol. Cell. Biol.* **14**, 7943–7952 (1994).
- G. E. Ayala, H. Dai, M. Powell, R. Li, Y. Ding, T. M. Wheeler, D. Shine, D. Kadmon, T. Thompson, B. J. Miles, M. M. Ittmann, D. Rowley, Cancer-related axonogenesis and neurogenesis in prostate cancer. *Clin. Cancer Res.* **14**, 7593–7603 (2008).
- N. Shah, S. Khurana, K. Cheng, J. P. Raufman, Muscarinic receptors and ligands in cancer. *Am. J. Physiol. Cell Physiol.* **296**, C221–C232 (2009).
- J. P. Raufman, J. Shant, G. Xie, K. Cheng, X. M. Gao, B. Shiu, N. Shah, C. B. Drachenberg, J. Heath, J. Wess, S. Khurana, Muscarinic receptor subtype-3 gene ablation and scopolamine butylbromide treatment attenuate small intestinal neoplasia in *Apc^{min/+}* mice. *Carcinogenesis* **32**, 1396–1402 (2011).
- C. Magnon, S. J. Hall, J. Lin, X. Xue, L. Gerber, S. J. Freedland, P. S. Frenette, Autonomic nerve development contributes to prostate cancer progression. *Science* **341**, 1236361 (2013).
- R. Pardal, M. F. Clarke, S. J. Morrison, Applying the principles of stem-cell biology to cancer. *Nat. Rev. Cancer* **3**, 895–902 (2003).
- N. Barker, M. Huch, P. Kujala, M. van de Wetering, H. J. Snippert, J. H. van Es, T. Sato, D. E. Stange, H. Begthel, M. van den Born, E. Danenberg, S. van den Brink, J. Korving, A. Abo, P. J. Peters, N. Wright, R. Poulosom, H. Clevers, *Lgr5⁺* stem cells drive self-renewal in the stomach and build long-lived gastric units in vitro. *Cell Stem Cell* **6**, 25–36 (2010).
- J. Ferlay, H. R. Shin, F. Bray, D. Forman, C. Mathers, D. M. Parkin, Estimates of worldwide burden of cancer in 2008: GLOBOCAN 2008. *Int. J. Cancer* **127**, 2893–2917 (2010).
- A. Jemal, M. M. Center, C. DeSantis, E. M. Ward, Global patterns of cancer incidence and mortality rates and trends. *Cancer Epidemiol. Biomarkers Prev.* **19**, 1893–1907 (2010).
- R. Håkanson, S. Vallgren, M. Ekelund, J. F. Rehfeld, F. Sundler, The vagus exerts trophic control of the stomach in the rat. *Gastroenterology* **86**, 28–32 (1984).
- J. Axelson, M. Ekelund, R. Håkanson, F. Sundler, Gastrin and the vagus interact in the trophic control of the rat oxyntic mucosa. *Regul. Pept.* **22**, 237–243 (1988).
- G. Lundegårdh, A. Ekborn, J. K. McLaughlin, O. Nyrén, Gastric cancer risk after vagotomy. *Gut* **35**, 946–949 (1994).
- S. Bahmanyar, W. Ye, P. W. Dickman, O. Nyrén, Long-term risk of gastric cancer by subsite in operated and unoperated patients hospitalized for peptic ulcer. *Am. J. Gastroenterol.* **102**, 1185–1191 (2007).
- P. Correa, C. Cuello, E. Duque, Carcinoma and intestinal metaplasia of the stomach in Colombian migrants. *J. Natl. Cancer Inst.* **44**, 297–306 (1970).
- M. Cassaro, M. Rugge, O. Gutierrez, G. Leandro, D. Y. Graham, R. M. Genta, Topographic patterns of intestinal metaplasia and gastric cancer. *Am. J. Gastroenterol.* **95**, 1431–1438 (2000).
- T. C. Wang, C. A. Dangler, D. Chen, J. R. Goldenring, T. Koh, R. Raychowdhury, R. J. Coffey, S. Ito, A. Varro, G. J. Dockray, J. G. Fox, Synergistic interaction between hypergastrinemia and *Helicobacter* infection in a mouse model of gastric cancer. *Gastroenterology* **118**, 36–47 (2000).
- J. G. Fox, T. C. Wang, Inflammation, atrophy, and gastric cancer. *J. Clin. Invest.* **117**, 60–69 (2007).
- P. Ericsson, R. Håkanson, J. F. Rehfeld, P. Norlén, Gastrin release: Antrum microdialysis reveals a complex neural control. *Regul. Pept.* **161**, 22–32 (2010).
- A. B. Rogers, N. S. Taylor, M. T. Whary, E. D. Stefanich, T. C. Wang, J. G. Fox, *Helicobacter pylori* but not high salt induces gastric intraepithelial neoplasia in B6129 mice. *Cancer Res.* **65**, 10709–10715 (2005).
- H. Tomita, S. Takaishi, T. R. Menheniott, X. Yang, W. Shibata, G. Jin, K. S. Betz, K. Kawakami, T. Minamoto, C. Tomasetto, M. C. Rio, N. Lerkowit, A. Varro, A. S. Giraud, T. C. Wang, Inhibition of gastric carcinogenesis by the hormone gastrin is mediated by suppression of *TF1* epigenetic silencing. *Gastroenterology* **140**, 879–891 (2011).
- S. Tu, G. Bhagat, G. Cui, S. Takaishi, E. A. Kurt-Jones, B. Rickman, K. S. Betz, M. Penz-Oesterreicher, O. Bjorkdahl, J. G. Fox, T. C. Wang, Overexpression of interleukin-1 β induces gastric inflammation and cancer and mobilizes myeloid-derived suppressor cells in mice. *Cancer Cell* **14**, 408–419 (2008).
- D. Dressler, F. Adib Saberi, Botulinum toxin: Mechanisms of action. *Eur. Neurol.* **53**, 3–9 (2005).
- P. Polakis, Drugging Wnt signalling in cancer. *EMBO J.* **31**, 2737–2746 (2012).
- F. Takahashi-Yanaga, M. Kahn, Targeting Wnt signaling: Can we safely eradicate cancer stem cells? *Clin. Cancer Res.* **16**, 3153–3162 (2010).
- M. Zöller, CD44: Can a cancer-initiating cell profit from an abundantly expressed molecule? *Nat. Rev. Cancer* **11**, 254–267 (2011).
- S. Takaishi, T. Okumura, S. Tu, S. S. Wang, W. Shibata, R. Vigneshwaran, S. A. Gordon, Y. Shimada, T. C. Wang, Identification of gastric cancer stem cells using the cell surface marker CD44. *Stem Cells* **27**, 1006–1020 (2009).
- J. Schuijers, H. Clevers, Adult mammalian stem cells: The role of Wnt, Lgr5 and R-spondins. *EMBO J.* **31**, 2685–2696 (2012).
- J. Chen, Y. Li, T. S. Yu, R. M. McKay, D. K. Burns, S. G. Kernie, L. F. Parada, A restricted cell population propagates glioblastoma growth after chemotherapy. *Nature* **488**, 522–526 (2012).
- S. Okabe, Y. Kodama, H. Cao, H. Johannessen, C. M. Zhao, T. C. Wang, R. Takahashi, D. Chen, Topical application of acetic acid in cyoreduction of gastric cancer. A technical report using mouse model. *J. Gastroenterol. Hepatol.* **27** (Suppl. 3), 40–48 (2012).
- P. Song, H. S. Sekhon, X. W. Fu, M. Maier, Y. Jia, J. Duan, B. J. Proskosil, C. Gravett, J. Lindstrom, G. P. Mark, S. Saha, E. R. Spindel, Activated cholinergic signaling provides a target in squamous cell lung carcinoma. *Cancer Res.* **68**, 4693–4700 (2008).
- C. B. Westphalen, S. Asfaha, Y. Hayakawa, Y. Takemoto, D. J. Lukin, A. H. Nuber, A. Brandtner, W. Setlik, H. Remotti, A. Muley, X. Chen, R. May, C. W. Houchen, J. G. Fox, M. D. Gershon, M. Quante, T. C. Wang, Long-lived intestinal tuft cells serve as colon cancer-initiating cells. *J. Clin. Invest.* **124**, 1283–1295 (2014).
- A. A. Gershon, J. Chen, M. D. Gershon, A model of lytic, latent, and reactivating varicella-zoster virus infections in isolated enteric neurons. *J. Infect. Dis.* **197** (Suppl. 2), S61–S65 (2008).
- N. Barker, H. Clevers, Leucine-rich repeat-containing G-protein-coupled receptors as markers of adult stem cells. *Gastroenterology* **138**, 1681–1696 (2010).
- M. Tatsuta, H. Yamamura, H. Iishi, M. Ichii, S. Noguchi, M. Baba, H. Taniguchi, Promotion by vagotomy of gastric carcinogenesis induced by *N*-methyl-*N*-nitro-*N*-nitrosoguanidine in Wistar rats. *Cancer Res.* **45**, 194–197 (1985).
- M. Tatsuta, H. Iishi, H. Yamamura, M. Baba, H. Taniguchi, Effects of bilateral and unilateral vagotomy on gastric carcinogenesis induced by *N*-methyl-*N*-nitro-*N*-nitrosoguanidine in Wistar rats. *Int. J. Cancer* **42**, 414–418 (1988).
- P. S. Frenette, S. Pinho, D. Lucas, C. Scheiermann, Mesenchymal stem cell: Keystone of the hematopoietic stem cell niche and a stepping-stone for regenerative medicine. *Annu. Rev. Immunol.* **31**, 285–316 (2013).
- E. R. Gross, M. D. Gershon, K. G. Margolis, Z. V. Gertsberg, R. A. Cowles, Neuronal serotonin regulates growth of the intestinal mucosa in mice. *Gastroenterology* **143**, 408–417.e2 (2012).
- T. Sato, J. H. van Es, H. J. Snippert, D. E. Stange, R. G. Vries, M. van den Born, N. Barker, N. F. Shroyer, M. van de Wetering, H. Clevers, Paneth cells constitute the niche for Lgr5 stem cells in intestinal crypts. *Nature* **469**, 415–418 (2011).
- D. W. Powell, I. V. Pinchuk, J. I. Saada, X. Chen, R. C. Mifflin, Mesenchymal cells of the intestinal lamina propria. *Annu. Rev. Physiol.* **73**, 213–237 (2011).
- H. F. Farin, J. H. Van Es, H. Clevers, Redundant sources of Wnt regulate intestinal stem cells and promote formation of Paneth cells. *Gastroenterology* **143**, 1518–1529.e7 (2012).
- D. Revesz, M. Tjernstrom, E. Ben-Menachem, T. Thorlin, Effects of vagus nerve stimulation on rat hippocampal progenitor proliferation. *Exp. Neurol.* **214**, 259–265 (2008).
- D. Cassiman, L. Libbrecht, N. Sinelli, V. Desmet, C. Deneff, T. Roskams, The vagal nerve stimulates activation of the hepatic progenitor cell compartment via muscarinic acetylcholine receptor type 3. *Am. J. Pathol.* **161**, 521–530 (2002).
- T. Aihara, T. Fujishita, K. Kanatani, K. Furutani, E. Nakamura, M. M. Taketo, M. Matsui, D. Chen, S. Okabe, Impaired gastric secretion and lack of trophic responses to hypergastrinemia in M₃ muscarinic receptor knockout mice. *Gastroenterology* **125**, 1774–1784 (2003).
- S. Salமான, S. M. Najafi, M. Rafipour, M. R. Arjomand, H. Shahheydari, S. Ansari, L. Kashkooli, S. J. Rasouli, M. S. Jazi, T. Minaei, Regulation of GSK-3 β and β -catenin by G α q in HEK293T cells. *Biochem. Biophys. Res. Commun.* **395**, 577–582 (2010).

47. E. R. Spindel, Muscarinic receptor agonists and antagonists: Effects on cancer. *Handb. Exp. Pharmacol.* 451–468 (2012).
48. J. P. Raufman, R. Samimi, N. Shah, S. Khurana, J. Shant, C. Drachenberg, G. Xie, J. Wess, K. Cheng, Genetic ablation of M₃ muscarinic receptors attenuates murine colon epithelial cell proliferation and neoplasia. *Cancer Res.* **68**, 3573–3578 (2008).
49. P. W. Veenboer, J. L. Bosch, Long-term adherence to antimuscarinic therapy in everyday practice: A systematic review. *J. Urol.* **191**, 1003–1008 (2014).
50. P. Song, H. S. Sekhon, A. Lu, J. Arredondo, D. Sauer, C. Gravett, G. P. Mark, S. A. Grando, E. R. Spindel, M₃ muscarinic receptor antagonists inhibit small cell lung carcinoma growth and mitogen-activated protein kinase phosphorylation induced by acetylcholine secretion. *Cancer Res.* **67**, 3936–3944 (2007).
51. H. Oshima, M. Oshima, Mouse models of gastric tumors: Wnt activation and PGE₂ induction. *Pathol. Int.* **60**, 599–607 (2010).
52. J. H. van Es, P. Jay, A. Gregorieff, M. E. van Gijn, S. Jonkheer, P. Hatzis, A. Thiele, M. van den Born, H. Begthel, T. Brabletz, M. M. Taketo, H. Clevers, Wnt signalling induces maturation of Paneth cells in intestinal crypts. *Nat. Cell Biol.* **7**, 381–386 (2005).
53. S. Fre, S. K. Pallavi, M. Huyghe, M. Laé, K. P. Janssen, S. Robine, S. Artavanis-Tsakonas, D. Louvard, Notch and Wnt signals cooperatively control cell proliferation and tumorigenesis in the intestine. *Proc. Natl. Acad. Sci. U.S.A.* **106**, 6309–6314 (2009).
54. L. Lehtii, N. W. Chi, S. Krauss, Tankyrases as drug targets. *FEBS J.* **280**, 3576–3593 (2013).

Acknowledgments: We thank A. Øverby, O. D. Røe, and J. E. Gronbech at Norwegian University of Science and Technology (NTNU) for valuable assistance and discussions; A. A. Diacou at Columbia University for extraction of enteric nervous system; and K. Takeuchi at Kyoto Pharmaceutical University for providing M₃KO mice. The microarray and part of the bioinformatics work were provided by Norwegian Microarray Consortium–NTNU, a national technology platform supported by Functional Genomics Programme (FUGE) of Research Council of Norway (RCN) and NTNU. **Funding:** Supported by the RCN (D.C.), Joint Programme of the Medical Faculty of NTNU and St. Olavs University Hospital, Liaison Committee between the Central Norway Regional Health Authority and NTNU (C.-M.Z.), U.S. NIH (grants 1U54CA126513, RO1CA093405, and RO1CA120979) (T.C.W.), Clyde Wu Family Foundation (T.C.W.), Mitsukoshi Health and Welfare Foundation (Y.H.), Japan Society for the Promotion of Science Postdoctoral

Fellowships for Research Abroad (Y.H.), and Uehara Memorial Foundation (Y.H.). Y.K., H.J., and G.T.A. are supported by Ph.D. fellowships from the FUGE of RCN, the European Union Seventh Framework Programme (FP7/2007–2013, no. 266408), and the St. Olavs Hospital, respectively. C.B.W. and M.Q. are supported by the Max Eder Program of the Deutsche Krebshilfe. C.B.W. is supported by the German Research Foundation. **Author contributions:** C.-M.Z. and Y.H. contributed equally to the design of the experiments, performance of the animal experiments and histology, the in vitro experiments, flow cytometry, and qRT-PCRs and contributed collection and analysis of the data. Y.K. performed the animal experiments (except for nos. 3 and 9 to 14 in table S1) and qRT-PCR arrays and contributed to collection and analysis of the data. A.F. and R.A.F. performed the bioinformatics analysis. S.M. and J.G.F. performed the pathological evaluation of mice. A.K.S. and V.B. performed the microarray experiments of mice and humans. G.T.A., H.J., and B.W.R. performed part of animal experiments. H.T. and A.H. performed the pathological evaluation of humans. C.B.W., M.Q., and H.T. performed some of the immunohistochemical analyses of mice and humans. Z.L. and M.D.G. performed the vagus nerve mapping. K.K. performed the analysis of human gastric stump cancer. T.C.W. and D.C. were joint senior authors; contributed to the study supervision, coordination, and performance of experiments; and wrote the manuscript. All authors contributed to the discussion of results and the preparation of the final manuscript. **Competing interests:** The authors declare that they have no competing interests. **Data and materials availability:** Mouse microarray data are available through Gene Expression Omnibus (GEO) database, accession no. GSE30295, and human data are in ArrayExpress, accession no. E-MTAB-1338.

Submitted 19 May 2014

Accepted 15 July 2014

Published 20 August 2014

10.1126/scitranslmed.3009569

Citation: C.-M. Zhao, Y. Hayakawa, Y. Kodama, S. Muthupalani, C. B. Westphalen, G. T. Andersen, A. Flatberg, H. Johannessen, R. A. Friedman, B. W. Renz, A. K. Sandvik, V. Beisvag, H. Tomita, A. Hara, M. Quante, Z. Li, M. D. Gershon, K. Kaneko, J. G. Fox, T. C. Wang, D. Chen, Denervation suppresses gastric tumorigenesis. *Sci. Transl. Med.* **6**, 250ra115 (2014).

Supplementary Materials for

Denervation suppresses gastric tumorigenesis

Chun-Mei Zhao, Yoku Hayakawa, Yosuke Kodama, Sureshkumar Muthupalani, Christoph B. Westphalen, Gøran T. Andersen, Arnar Flatberg, Helene Johannessen, Richard A. Friedman, Bernhard W. Renz, Arne K. Sandvik, Vidar Beisvag, Hiroyuki Tomita, Akira Hara, Michael Quante, Zhishan Li, Michael D. Gershon, Kazuhiro Kaneko, James G. Fox, Timothy C. Wang,* Duan Chen*

*Corresponding author. E-mail: duan.chen@ntnu.no (D.C.); tcw21@columbia.edu (T.C.W.)

Published 20 August 2014, *Sci. Transl. Med.* 6, 250ra115 (2014)

DOI: 10.1126/scitranslmed.3009569

The PDF file includes:

Materials and Methods

Fig. S1. Flowchart showing the animal study design.

Fig. S2. Anterior UVT in mice.

Fig. S3. Body weight of male and female INS-GAS mice after surgery.

Fig. S4. Thickness of the gastric oxyntic mucosa after surgery in INS-GAS mice.

Fig. S5. Pathological scores for the stomach after surgery in INS-GAS mice.

Fig. S6. Pathological scores for the stomach after Botox injection in INS-GAS mice.

Fig. S7. Wnt signaling in INS-GAS mice compared with wild-type mice.

Fig. S8. Altered signaling pathways after vagotomy in INS-GAS mice.

Fig. S9. Wnt and Notch signaling pathways after vagotomy in INS-GAS mice.

Fig. S10. Immunostaining of CD44 after vagotomy in INS-GAS mice.

Fig. S11. Numbers of CD44-immunoreactive cells after Botox treatment ± vagotomy in INS-GAS mice.

Fig. S12. Tumor regeneration in the stomach after vagotomy in INS-GAS mice.

Fig. S13. Wnt signaling KEGG pathway in M₃KO mice compared with wild-type mice.

Fig. S14. Altered signaling pathways in human gastric cancer tissue compared with adjacent noncancerous tissue.

Fig. S15. Gastric stump cancer after distal gastrectomy with or without vagotomy.

Fig. S16. Effect of 5-FU and oxaliplatin in INS-GAS mice.

Table S1. Animal experimental groups.

Table S2. Cohorts of gastric cancer patients.

Table S3. List of qRT-PCR primers used in this study.

Supplementary Materials and Methods

Animals

The insulin-gastrin (INS-GAS) transgenic mice were generated by Dr. T.C. Wang (18), and imported to Norway by Dr. D. Chen for these studies. Animals were further bred through sibling mating for more than 20 generations. 829 INS-GAS mice have been examined during the past 9 years. The percentage of the mice without preneoplastic lesions was 3.7% at 6 months of age, and the prevalence of spontaneous gastric cancer increased from 75% (at the beginning of this study in Jan. 2005) to 100% (May 2013) at 12 months of age without an additional infection with *Helicobacter pylori*. 187 INS-GAS mice were examined at 1 to 20 months of age during 2005, and 61 mice were found to have gastric tumors after 9 months of age (see Fig. 1A: the tumor prevalence at the lesser or greater curvature of the stomach). During 2012, 139 INS-GAS mice were examined at 12 months of age and all mice had gastric tumors. M₃KO mice were obtained from Dr. Koji Takeuchi at Kyoto Pharmaceutical University (45). M₃KO mice had higher water intake than age- and sex-matched wild type mice (14.62±1.71 vs. 6.48±1.00 mL/100 g body weight/24 hours, Means ± SEM (N=8), *p* = 0.01 (Student's *t* test). The chemically-induced gastric cancer model was established according to our previous report (22). In brief, mice were exposed to N-Methyl-N-nitrosourea (MNU, Sigma Chemicals), which was dissolved in distilled water at a concentration of 240 ppm and freshly prepared twice per week for administration in drinking water in

light-shielded bottles *ad libitum*. Starting at 4 weeks of age, mice were given drinking water containing MNU on alternate weeks for a total of 10 weeks. *H. pylori* infection was induced in H^+/K^+ -ATPase-IL-1 β mice (23) by inoculation with pre-mouse Sydney strain 1 [PMSS1]). Three inocula (0.2 mL of *Hp*, 10^{10} colony-forming units/mL) were delivered every other day by oral gavage using a sterile gavage needle.

In the present study, animals were housed 3-4 mice per cage on wood chip bedding with a 12-hour light/dark cycle, room temperature of 22°C and 40-60% relative humidity. INS-GAS mice and FVB wild-type (WT) mice were housed at the standard housing conditions in a specific pathogen-free environment. M_3 KO mice, *Hp*-infected H^+/K^+ -ATPase-IL-1 β mice, and WT controls (C57BL/6 mice, Taconic, Denmark) were housed in a guaranteed animal facility at Comparative Medicine Core Facility at Norwegian University of Science and Technology. All the mice had free access to tap water and standard pellet food (RM1 801002, Scanbur BK AS). Animal experiments were approved by the Norwegian National Animal Research Authority (Forsøksdyrutvalget, FDU) and by the Columbia University Institutional Animal Care and Use Committee (IACUC).

Experimental designs

581 mice were divided into 14 experimental groups (Table S1). In each experiment, mice were randomly divided into different subgroups. The animals, samples, and treatments were coded until the data were analyzed.

In the 1st experiment, 107 INS-GAS mice underwent bilateral truncal vagotomy with pyloroplasty (VTPP) (6 males, 19 females), pyloroplasty alone (PP) (7 males, 18 females), unilateral anterior truncal vagotomy (UVT) (11 males, 19 females), or sham operation (11 males, 16 females) at 6 months of age. Six months after surgery (at 12 months of age), the animals were euthanized, and the anterior and posterior parts of the stomachs were collected for histopathological and immunohistochemical analyses.

In the 2nd experiment, 20 WT mice (FVB, the same genetic background as INS-GAS mice) were exposed to MNU for one week every other week for 5 cycles (10 weeks). At 3.5 months of age, half of the MNU-treated mice underwent VTPP and the other half underwent a sham operation (PP). All the mice were euthanized at 13 months of age, and the stomachs were examined macroscopically and collected for histopathological analysis.

In the 3rd experiment, 24 H⁺/K⁺-ATPase-IL-1 β mice (14 males and 10 females, backcrossed to C57BL/6 for 10 generation) were inoculated with *Hp* at 3.5 months of age. At 12 months of age, half of the infected mice underwent UVT and the other half underwent a sham operation (laparotomy). All the mice were euthanized 6 months later. The stomachs were examined macroscopically and collected for histopathological analysis.

In the 4th experiment, 16 INS-GAS mice (5 males and 11 females) at 6 months of age underwent unilateral Botox treatment and were euthanized at 12 months of age. The anterior and posterior parts of the stomachs were collected for histopathological analysis.

In the 5th experiment, 64 INS-GAS mice at 8 months (7 males and 10 females), 10 months (6 males and 8 females) and 12 months (6 males and 6 females) of age underwent UVT, and 21 age-matched mice (8 males and 13 females) had no surgery. At 18 months of age, all surviving mice including 12 (6 males and 6 females) from the 8-month group, 9 from the 10-month group (3 males and 6 females), 8 from the 12-month group (4 males and 4 females), and 10 from the un-operated group (4 males and 6 females) were euthanized, and the anterior and posterior parts of the stomachs were collected for histopathological analysis and genome-wide gene expression profiling analysis. Survival analysis was also performed.

In the 6th experiment, 26 INS-GAS mice at 12 months of age underwent Botox treatments (only anterior or both anterior and posterior sides of the stomach with or without UVT) or vehicle injection (both anterior and posterior sides of the stomach). Mice were euthanized at 14 months of age. Both the anterior and posterior parts of the stomachs were collected for histopathological analysis.

In the 7th experiment, 133 INS-GAS mice at 12-14 months of age received no treatment (6 males and 6 females), saline (5 males and 5 females), 5-fluorouracil (5-FU) (5 males and 5 females), oxaliplatin (5 males and 8 females), saline + unilateral Botox treatment (4 males

and 6 females), unilateral Botox treatment + 5-FU (4 males and 6 females), unilateral Botox treatment + oxaliplatin (6 males and 7 females), sham operation (laparotomy) + 5-FU + oxaliplatin (6 males and 9 females), unilateral Botox treatment + 5-FU + oxaliplatin (11 males and 13 females), or UVT+ 5-FU + oxaliplatin (6 males and 10 females). Denervation treatment was applied to only half of the stomach, such that the non-denervated half of the stomach in each animal served as a control, either as chemotherapy only or as an untreated control. All mice were euthanized 2 months after starting the treatments, except for mice that died before the end of study, and both the anterior and posterior parts of the stomachs were collected for histopathological analysis. Survival analysis was also performed.

In the 8th experiment, 16 INS-GAS mice at 6 months of age underwent UVT and were euthanized at 2 months (1 male and 4 females), 4 months (2 males and 3 females), or 6 months (2 males and 4 females) postoperatively. The anterior and posterior parts of the stomachs were collected for genome-wide gene expression profiling.

In the 9th experiment, 44 INS-GAS mice at 12-14 months of age received saline (3 males and 3 females), 5-FU + oxaliplatin (5 males and 8 females), darifenacin (6 males and 6 females), or a combination of 5-FU + oxaliplatin and darifenacin (8 males and 5 females). Two months after starting the treatments, the mice were euthanized, and both the anterior and posterior parts of the stomachs were collected for histopathological analysis.

In the 10th experiment, both INS-GAS mice (6 males and 6 females) and WT mice (10 males and 10 females) were subjected either to UVT or no treatment. Six months after surgery (at 12 months of age), the animals were euthanized and the anterior and posterior parts of the stomachs were collected for gene expression analysis.

In the 11th experiment, 12 MNU-treated mice (6 males and 6 females) were subjected to PP or VTPP at 6 months of age and euthanized 4 months later. The stomachs were collected for qRT-PCR analysis.

In the 12th experiment, 7 M₃KO mice (4 males and 3 females) and 13 WT mice (5 males and 8 females) (C57BL/6, the same genetic background as M₃ KO mice) were exposed to MNU and euthanized at 11 months of age. The stomachs were examined macroscopically and were collected for histopathological analysis.

In the 13th experiment, 37 mice (20 males, 17 females) at 12-18 months of age underwent a topical application of acetic acid on the anterior side of the stomach with or without simultaneous UVT and were euthanized 1 week (5 males, 7 females), 2 weeks (3 males, 9 females), or 3 weeks (12 males, 1 female) later, and the anterior parts of the stomachs were collected for histopathological analysis.

In the 14th experiment, 10 Lgr5-GFP mice (all males) were treated with MNU at 2 months of age, subjected to PP or VTPP at 19 weeks of age, and euthanized at 25 weeks of age.

Animal surgery

All surgical procedures were performed under isoflurane inhalation anesthesia (2-3 %), with buprenorphine (0.1 mg/kg subcutaneously) given as postoperative analgesia. The abdominal cavity was accessed through a midline incision. The sham operation consisted of a laparotomy with mild manipulation of organs, including identification of the vagus nerve. PP was done by longitudinal incision of the pyloric sphincter followed by transverse suturing. VTPP was performed by subdiaphragmatic dissection of both the anterior and posterior vagal trunks and simultaneous PP to prevent post-vagotomy delayed gastric emptying. In UVT, only the anterior truncal vagus nerve was cut (Fig. S2), leading to a specific vagal denervation of the anterior aspects of the stomach, with preserved pyloric function making PP unnecessary. Sample collection was done under inhalation anesthesia as described, and the animals were euthanized by exsanguination while still under anesthesia.

Botox treatment

Botox 100 U (Botox Allergan Inc.) was dissolved in 0.9% cold saline and 1% methylene blue (to visualize the injection), achieving a concentration of 0.25 U of Botox/mL. The Botox solution was injected subserosally along the greater curvature into the anterior (unilateral Botox treatment) or both anterior and posterior sides (bilateral Botox treatment) of the stomach (only the corpus area where tumor developed) at the dose of 0.05 U/mouse (0.2

mL/mouse) or 0.1 U/mouse (0.4 mL/mouse), respectively, once per month until the end of the study. In the control group, the vehicle solution was prepared with 0.9% saline and 1% methylene blue and injected into both anterior and posterior sides of the stomach (only the corpus area where tumor developed) at a volume of 0.4 mL/mouse.

Chemotherapy and M₃ receptor antagonist treatment

5-Fluorouracil (5-FU, Flurablastin, Pfizer, Inc.) was diluted in saline and given at a dose of 25 mg/kg in a volume of 1 mL. Oxaliplatin (Hospira, Inc.) was diluted in saline and given at 5 mg/kg in 1 mL. Combination of 5-FU (25 mg/kg in 0.5 mL) and oxaliplatin (5 mg/kg in 0.5 mL) was given at the same time, but the drugs were injected separately. Chemotherapy was given by intraperitoneal injection weekly in 2 cycles, namely 3 injections in the 1st month (starting one week after the 1st Botox, UVT, or the 1st osmotic mini-pump implantation), and 3 injections in the 2nd month (starting at one week after the 2nd Botox, no UVT, or the 2nd mini-pump). Age- and sex-matched mice received intraperitoneal injection of saline (1 mL) as controls. The injection needle was 27 G. The dosages and regimens were made based on our pilot experiments for selecting the doses. There was no effect on tumor size by 5-FU or oxaliplatin alone (Fig. S16).

Darifenacin hydrobromide (Santa Cruz Biotechnology) was given at a dose of 1 mg/kg/h for 2 months via an osmotic mini-pump (ALZET 2006) as reported previously (48).

Tumor regeneration model

Topical application of acetic acid was found to promptly cause necrosis in the tumor tissue in INS-GAS mice. Under isoflurane anesthesia, the stomach was exposed through a midline abdominal incision, and 60% acetic acid was topically applied to the serosa of the anterior side of the stomach for 60 seconds using a 5 mm internal diameter cylindrical metal mold. In the experiment combining acetic acid-induced necrotic ulcers with UVT, the mice underwent acetic acid application during the UVT surgery.

Pathological and immunohistochemical analyses

The stomachs were removed, opened along the greater curvature, washed in 0.9% NaCl, and pinned flat on a petri-dish-silicone board. Each stomach was photographed digitally; the tumor profiles in both anterior and posterior sides of the stomach were drawn separately and subjected to morphometric analysis of the volume density (expressed as the percentage of glandular volume occupied by the tumor) using point-counting technique with a test grid comprised of a 1.0 cm square lattice. This grid was placed over each photograph (40 x 30 cm²), and the numbers of test points overlying the tumor and gastric glandular area were determined. The samples for histology comprised multiple linear strips along the greater curvature of the stomach wall, extending from the squamocolumnar junction through the

antrum. Samples were fixed in 4% formaldehyde for 8-12 hours at room temperature and embedded in paraffin. Sections (4 μ m thick) were stained with hematoxylin and eosin. Pathological evaluation was performed by comparative pathologists and a histologist who were blinded to the sample source. The gastric lesions were scored on an ascending scale from 0 to 4, using criteria adopted from previous reports (21). Inflammation scoring were assigned for patchy infiltration of mixed leukocytes in mucosa and/or submucosa (1), multifocal-to-coalescing leukocyte infiltration not extended below submucosa (2), marked increase in leukocytes with lymphoid follicles +/- extension into tunica muscularis (3), or effacing transmural inflammation (4). The epithelial defects were defined as gland dilatation, surface erosions and gland atrophy, and ulceration and fibrosis. Immunohistochemistry was performed using a DAKO AutoStainer (Universal Staining System with DAKO EnVision System, Dako). Antibodies used were Ki67 (1:100; code M7249, Dako), PCNA (1:100, code M0879, Dako), CD44 (1:100, code 550538, BD Pharmingen), CD44V6 (1:200, code AB2080, Millipore), PGP9.5 (1:1000, code Z5116, Dako, and code 7863-0504, AbD Serotec), peripherin (1:500, code AB1530, Millipore), β -catenin (1:500, code 610654, BD Transduction Laboratories), Alexa Fluor 488 Phalloidin (1:200, code A12379, Life Technologies), Alexa Fluor 555 Goat Anti-Rabbit IgG (H+L)(1:200, code A21428, Life Technologies). Cellular proliferation is expressed as the number of Ki67 or PCNA immunoreactive cells/gland. There was no difference between the two markers between two

labs (TW and DC). Slides were visualized on a Nikon TE2000-U and representative microhistophotos were taken. Positive-stained cells with nuclei were counted only in dysplastic glands, with least 50 glands counted per animal in a blinded fashion, and results are expressed as numerical densities (number of cells per gland, number of cells per 10 glands or per object field). Positive-stained nerves were quantitated by ImageJ software and are expressed as positive area per total mucosal area.

Vagus nerve fibers and terminals in the mouse stomach traced with carbocyanine dye (DiI)

The esophagus, diaphragm and stomach were removed from adult mice and fixed for 3 days with formaldehyde. DiI crystals were placed on the anterior and posterior thoracic vagal trunks about 1 cm above the diaphragm, which was left undisturbed. The preparation was incubated at 37°C in PBS containing 0.5% sodium azide in a sealed container for 3 months. After incubation, the stomach was opened along the greater curvature, the mucosa and submucosa were removed, and the preparations were mounted, serosal side up, in buffered glycerol for microscopic examination. DiI fluorescence was viewed with a Leica CTR6000 microscope equipped with a cooled CCD camera and computer assisted video imaging. The entire gastric wall was scanned with a 2.5x objective, and a montage was made from the resulting images. In order to observe the density of DiI-labeled vagal fibers within the

myenteric plexus, additional images were obtained at higher magnification in the lesser curvature close to the esophagogastric junction and in the greater curvature. The density of DiI-labeled fibers was estimated by point counting technique. A test system comprising a 1.0 cm square lattice was placed over each photograph, and the numbers of test points overlying the DiI-labeled fibers and the visual field were determined.

RNA isolation, gene expression profiling by microarray, qRT-PCR arrays and qRT-PCR in mice and humans

The collected mouse and human stomach samples were kept frozen at -80°C until further processing. Total RNA from the frozen stomach samples was isolated and purified using an Ultra-Turrax rotating-knife homogenizer and the mirVana miRNA Isolation Kit (AM1560, Ambion) according to the manufacturer's instructions. Concentration and purity of total RNA were assessed using a NanoDrop photometer (NanoDrop Technologies, Inc.). The A260/280 ratios were 2.05 ± 0.01 for mouse samples and 1.96 ± 0.10 for human samples (mean \pm SEM). RNA integrity was assessed using a Bioanalyzer (Agilent Technologies) and found satisfactory, with RNA integrity number (RIN) values 9.1 ± 0.1 for mouse samples, and 8.7 ± 0.9 for human samples (means \pm SEM). The microarray gene expression analysis followed standard protocols, analyzing 300 ng total RNA per sample with the Illumina MouseWG-6 and HumanHT-12 Expression BeadChips (Illumina). Microarray data were confirmed by

qRT-PCR array (RT² Profiler PCR Array, SABiosciences) (StepOnePlus™, Applied Biosystems). Mouse microarray data were deposited in the Gene Expression Omnibus (GEO accession no. GSE30295), and human data in ArrayExpress (accession no. E-MTAB-1338). Longitudinal strips of gastric tissue from the anterior wall as well as the posterior wall were harvested and snap-frozen in dry ice and kept in a -80°C freezer until processed for analysis. Total RNA was extracted with Nucleospin RNA II kit (Clontech), and cDNA was synthesized by Superscript III First-strand Synthesis System for RT-PCR (Invitrogen). See Table S3 for primer sequences used. Expression levels of indicated genes were quantified by real-time PCR assays with SYBR Green dye and the Applied Biosystems 7300 Real Time PCR System.

Fluorescence-activated cell sorting (FACS)

Single epithelial cells were isolated from *Lgr5*-GFP mouse stomachs. Isolated crypts were dissociated with TrypLE Express (Invitrogen) including 1 mg/ml DNase I (Roche Applied Science) for 10 minutes at 37°C. Dissociated cells were passed through a 20- μ m cell strainer, washed with 2% FBS/PBS, and sorted by FACS (BD FACSAria Cell Sorter III). Viable single epithelial cells were gated by forward scatter, side scatter and a pulse-width parameter, and negative staining for propidium iodide. Cells expressing high and low levels of GFP and

GFP-negative cells were sorted separately, and RNA was isolated by using RNAqueous-Micro Kit (Ambion).

***In vitro* culture system**

Wild-type (WT), Ubiquitin C-green fluorescent protein (UBC-GFP), or Gt(ROSA)26Sortm4(ACTB-tdTomato,-EGFP)Luo/J mice (The Jackson laboratory) were used for *in vitro* culture. Gastric gland isolation and culture were performed as described previously (9), with minor modifications. Stomachs removed from WT and M₃KO mice were opened longitudinally, chopped into approximately 5 mm pieces, and incubated in 8 mM EDTA in PBS for 60 minutes on ice. The tissue fragments were vigorously suspended, yielding supernatants enriched in gastric glands. Gland fractions were centrifuged at 900 rpm for 5 minutes at 4°C and diluted with advanced DMEM/F12 (Invitrogen) containing B27, N2, 1 μ M n-Acetylcysteine, 10 mM HEPES, penicillin/streptomycin, and Glutamax (all Invitrogen). Glands were embedded in extracellular matrix (Fisher Bioservices/NCI Frederick Central Repository) and 400 crypts/well were seeded on pre-warmed plates. Advanced DMEM/F12 medium containing 50 ng/mL EGF, 100 ng/mL Noggin, and 1 μ g/mL R-spondin1 was applied. Wnt3a (PeproTech) was added at 100 ng/mL when indicated. Growth factors were added every other day, and the entire medium was changed twice a week. Passage was performed at day 7 as described previously (9). Mouse primary neuronal cells were prepared following the protocol described previously (33). Neuronal cells were

mixed with extracted gastric crypts in the extracellular matrix at the ratio of crypt:neuron 1:5. The enteric nervous system was isolated from guinea pigs as described previously (34). Botox, scopolamine hydrochloride, and pilocarpine hydrochloride (Sigma) were dissolved in PBS and added in the cultured medium every other day. The images of gastric organoids were acquired using fluorescent microscopy (Nikon, TE2000-U) and two-photon microscopy (Nikon, AIRMP). Isolation of mRNA from cultured organoids was performed with a NucleoSpin RNA XS kit (Clontech Laboratories Inc.) according to manufacturer's instructions. The first-strand complementary DNA was synthesized using the ImProm-II Reverse Transcription System (Promega). Amplification was performed using the ABI PRISM 7300 Quantitative PCR System (Applied Biosystems).

Patients and methods

Three cohort studies were included (Table S2). In the 1st study, human stomach specimens (both tumors and the adjacent non-tumor tissues) were taken immediately after gastrectomy from 17 patients during 2005 to 2010 at St. Olav's University Hospital, Trondheim, Norway for gene expression profiling analysis. All patients were diagnosed histologically as primary gastric carcinoma of stage I-IV. 10 of 17 patients were *H. pylori* positive at the time of surgery. In the 2nd study, human stomach tissues were obtained from 120 gastric cancer patients who underwent curative surgical resection from 2001 to 2008 at Gifu University

Hospital, Gifu, Japan. All patients were diagnosed histologically as primary gastric carcinoma of stage II, III, or IV. Immunohistochemical analysis of the nerve density was performed with PGP9.5 antibody. Low and high expression of PGP9.5 were defined with respect to the median of the volume density of PGP9.5. In the 3rd study, clinical data of 37 patients with gastric stump cancer (GSC) who had received distal gastrectomy with or without vagotomy during 1962 to 1995 at the National Cancer Center Hospital East, Chiba, Japan were evaluated. GSC was defined as gastric cancer that occurred \geq 5 years (from 5 to 36 years) after curative distal gastrectomy, regardless of the original benign or malignant disease. GSC included in this study was adenocarcinoma infiltrating the mucosal or submucosal layer. The tumor location was recorded according to the recommendation by the Japanese Gastric Cancer Association: anterior or posterior wall, or lesser or greater curvature (Fig. S15). All the study protocols were approved by the ethics committees in Japan and Norway, and written informed consent was obtained from patients.

Data analysis and statistics

Values were expressed as means \pm SEM. Pairwise comparisons between experimental groups and between anterior and posterior sides of the stomach were performed with the paired and unpaired *t*-test as appropriate. All tests were two sided with a significance cutoff of 0.05. Comparisons between more than 2 groups were performed by ANOVA, followed by

Dunnett's test or Tukey's test as appropriate. Comparisons with categorical independent variables were performed using Fisher's exact test. Kaplan-Meier survival curves were calculated and were analyzed by the Cox proportional hazard method. Tumor prevalence/incidence was analyzed by Fisher's exact test. Affymetrix microarray data were normalized using RMA, and Illumina microarray data was analyzed using Lumi. Both qRT-PCR and microarray data were analyzed on the \log_2 scale. The significance of differential expression of qRT-PCR data was analyzed using parametric frequentist statistics, and microarray data were analyzed using the empirical Bayesian method implemented in Limma. Gene expression profiles from both microarray and qRT-PCR were analyzed independently by a paired robust *t*-test for mouse samples or a paired *t*-test for human samples. Paired *t*-statistics were computed by fitting a linear robust or non-robust regression to the anterior and posterior stomach samples within each mouse or to the cancer and the adjacent non-cancerous tissue samples within each patient. For microarray data, transcripts with Benjamini-Hochberg false discovery rates less than 0.05 were considered to be differentially expressed. Regulated KEGG (Kyoto Encyclopedia of Genes and Genomes) pathways were identified using Signaling Pathway Impact Analysis. All of the above calculations were performed in the R/Bioconductor software environment.

Supplementary figures and tables

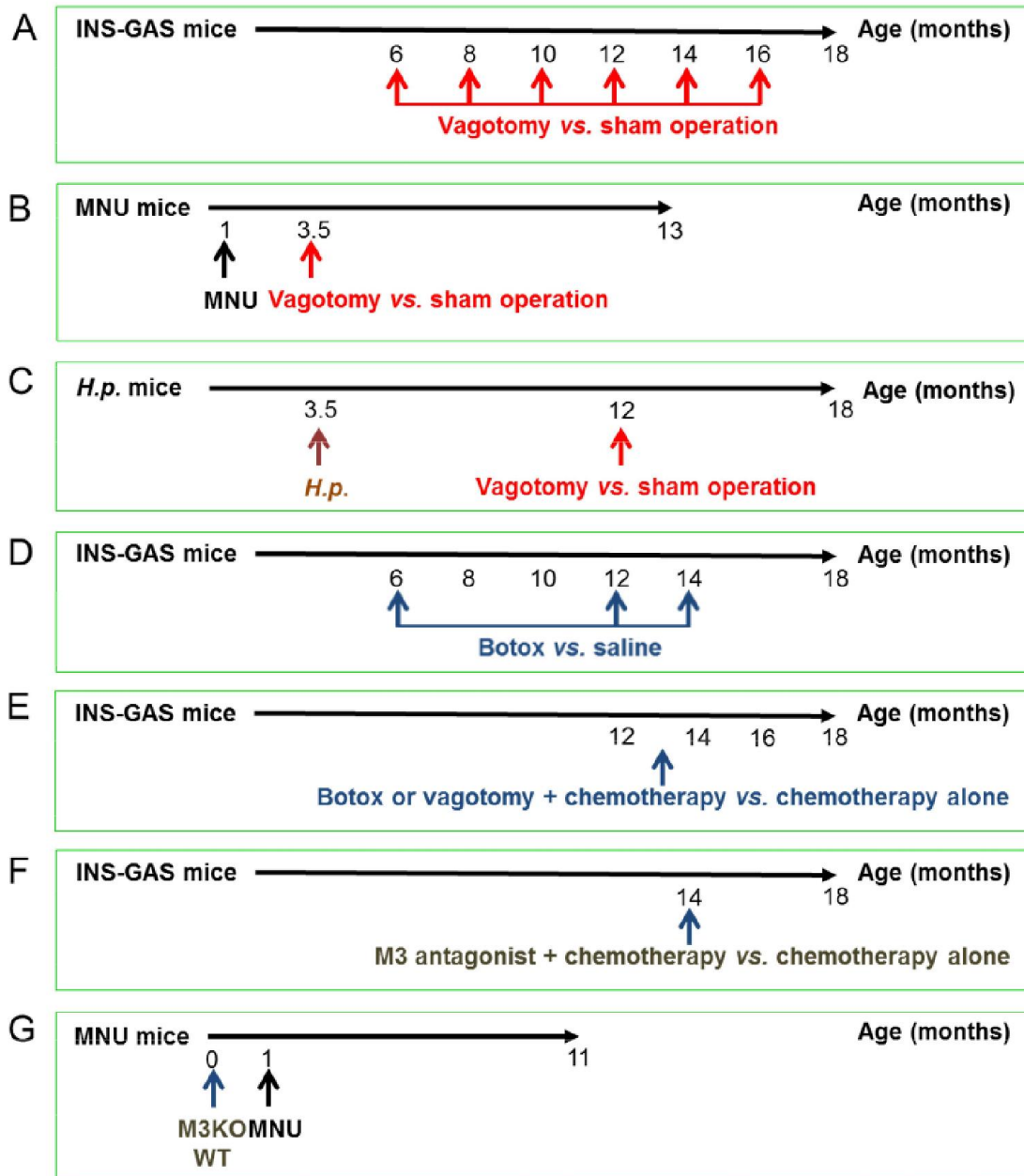


Fig. S1. Flowchart showing the animal study design.

□

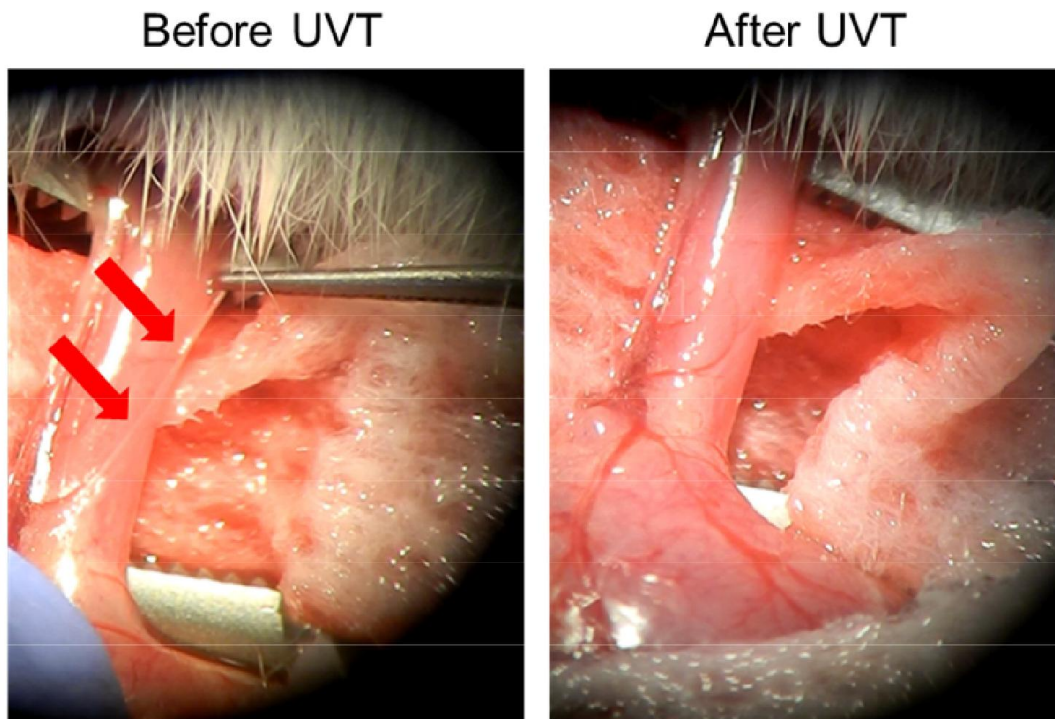


Figure S2: Anterior UVT in mice. Photographs showing dissected vagus nerve (indicated by arrows) before and after anterior unilateral truncal vagotomy (UVT) are shown.

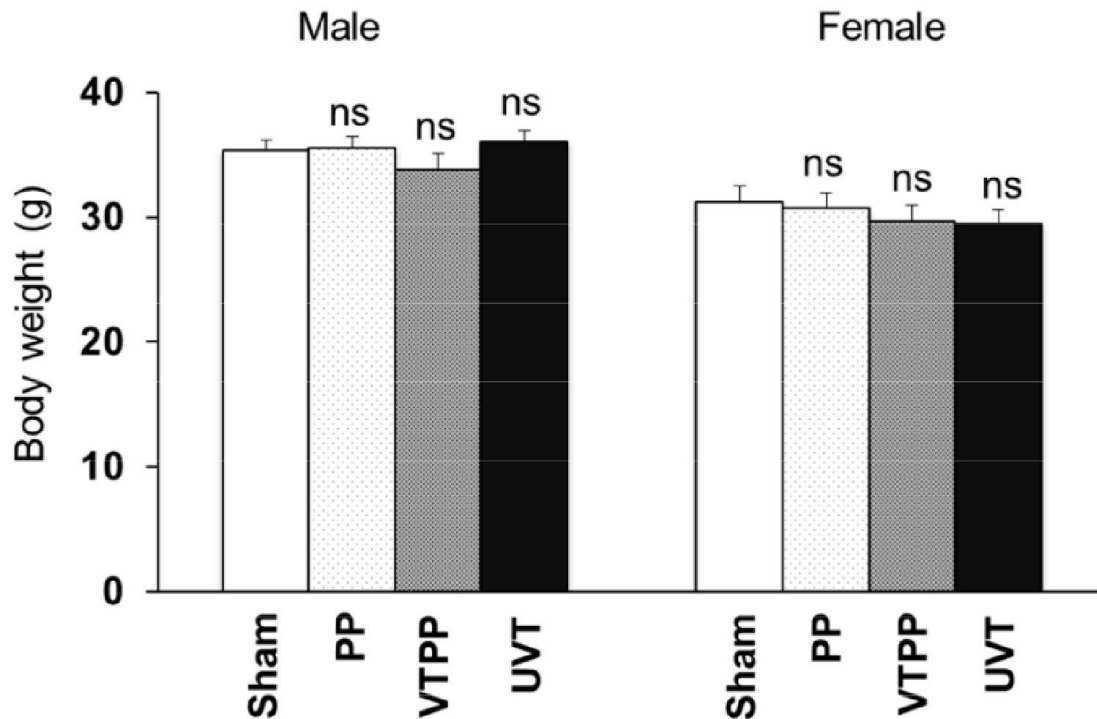


Figure S3: Body weight of male and female INS-GAS mice after surgery. Body weight of sham (Sham), pyloroplasty (PP), bilateral vagotomy with pyloroplasty (VTPP), and anterior unilateral vagotomy (UVT)-operated INS-GAS mice at 12 months of age (6 months postoperatively). Means \pm SEM. ns: not significantly different between Sham ($N = 11$ males, 16 females) and PP ($N = 7$ males, 18 females), VTPP ($N = 6$ males, 19 females), or UVT ($N = 11$ males, 19 females) (Dunnett's test).

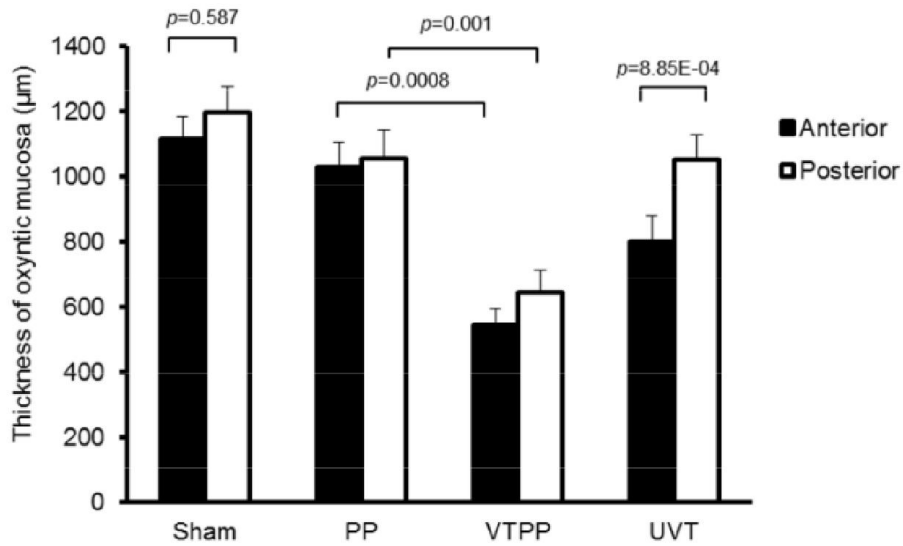


Figure S4: Thickness of the gastric oxyntic mucosa after surgery in INS-GAS mice. Thickness of the oxyntic mucosa in sham (Sham), pyloroplasty (PP), bilateral vagotomy with pyloroplasty (VTPP), and anterior unilateral vagotomy (UVT)-operated INS-GAS mice at 12 months of age (6 months postoperatively). Means \pm SEM. Tukey test: between PP ($N = 25$) and VTPP ($N = 25$). Paired t test: between anterior vs. posterior sides within Sham ($N = 27$) and UVT ($N = 30$).

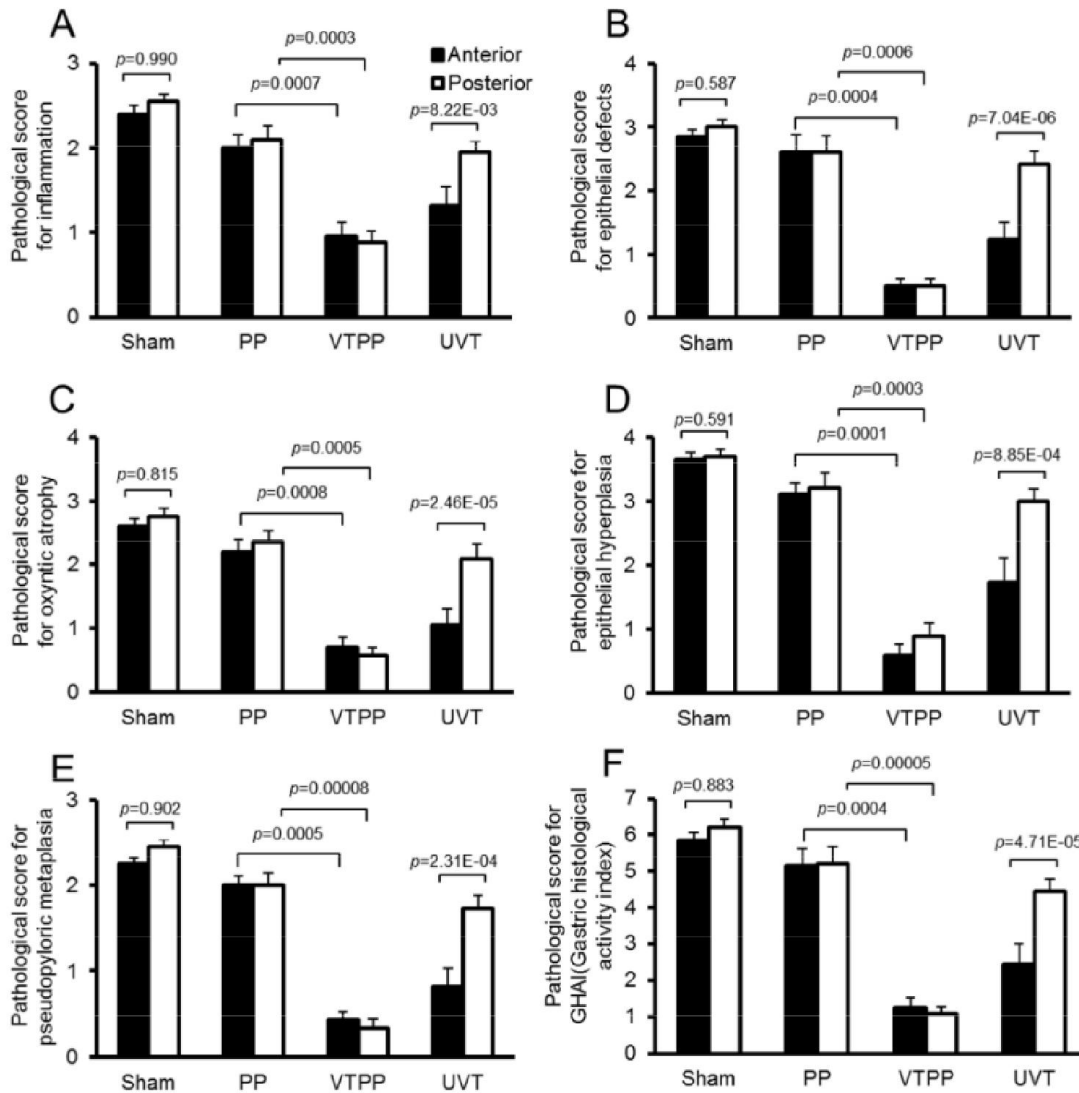


Figure S5: Pathological scores for the stomach after surgery in INS-GAS mice. Pathological scores for inflammation (A), epithelial defects (B), oxyntic atrophy (C), epithelial hyperplasia (D), pseudopyloric metaplasia (E), and GHAI (gastric histological activity index) (F) in sham (Sham), pyloroplasty (PP), bilateral vagotomy with pyloroplasty (VTPP), and anterior unilateral vagotomy (UVT)-operated INS-GAS mice at 12 months of age (at 6 months after surgery). Means \pm SEM. Tukey test: between PP ($N = 25$) and VTPP ($N = 25$). Paired t test:

between anterior vs. posterior sides within Sham ($N = 27$) and UVT ($N = 30$).

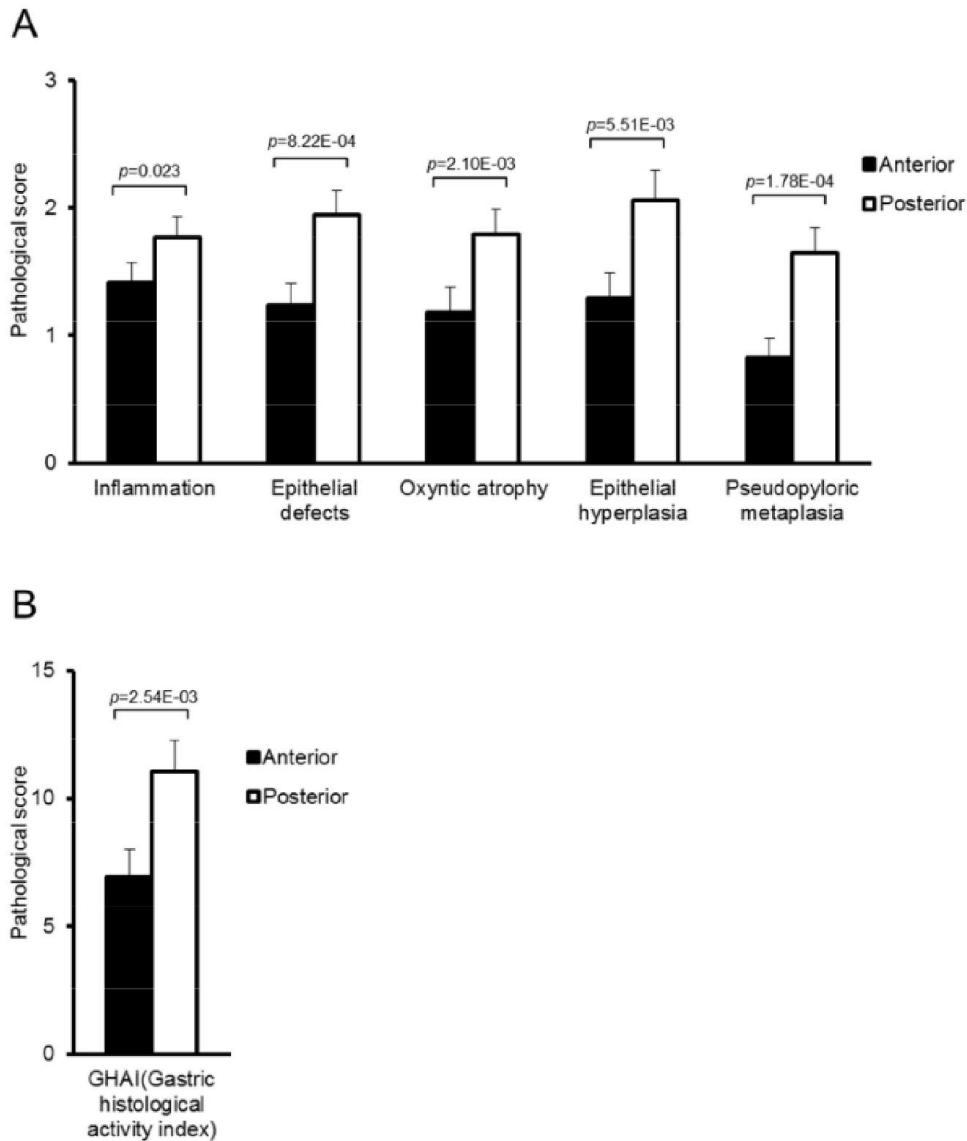


Figure S6: Pathological scores for the stomach after Botox injection in INS-GAS mice. Pathological scores for inflammation, epithelial defects, oxyntic atrophy, epithelial hyperplasia, pseudopyloric metaplasia (A), and GHAI (gastric histological activity index) (B) in Botox-injected (in anterior side of the stomach) INS-GAS mice at 12 months of age (monthly Botox injection starting at 6 months of age). Means \pm SEM ($N = 16$). Paired t test between anterior vs. posterior sides.

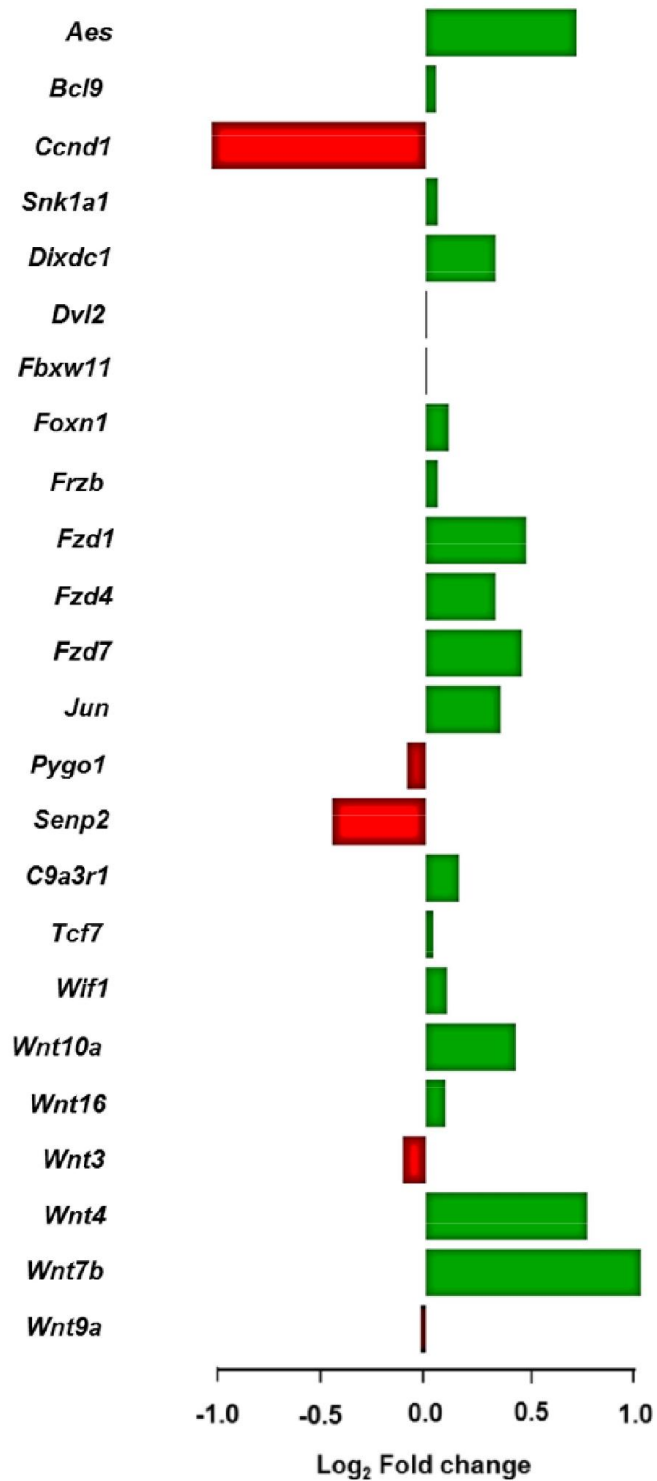


Figure S7: Wnt signaling in INS-GAS mice compared with wild-type mice. Fold changes of

Wnt-related genes: upregulated (indicated by red) and downregulated (green).

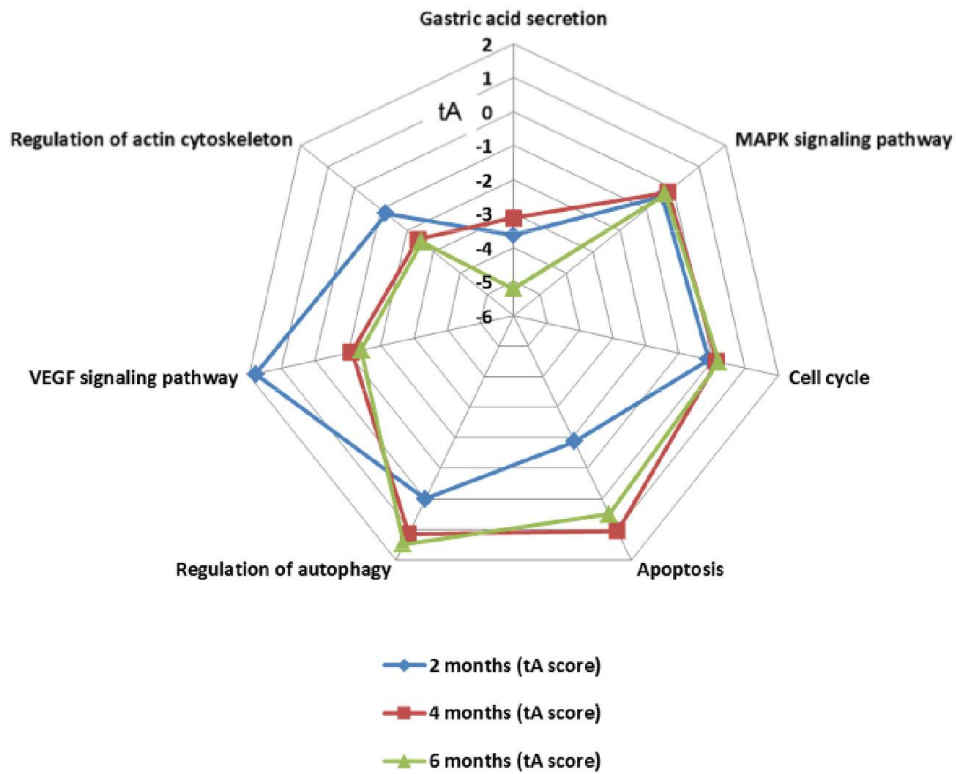


Figure S8: Altered signaling pathways after vagotomy in INS-GAS mice. Altered signaling pathways involved gastric acid, MAPK signaling, and tissue homeostasis at 2 (blue), 4 (green), and 6 (red) months in the anterior oxyntic mucosa of the stomach after anterior unilateral vagotomy compared with posterior side. tA score: -4 to 6. tA score>0: activation; tA score<0: inhibition.

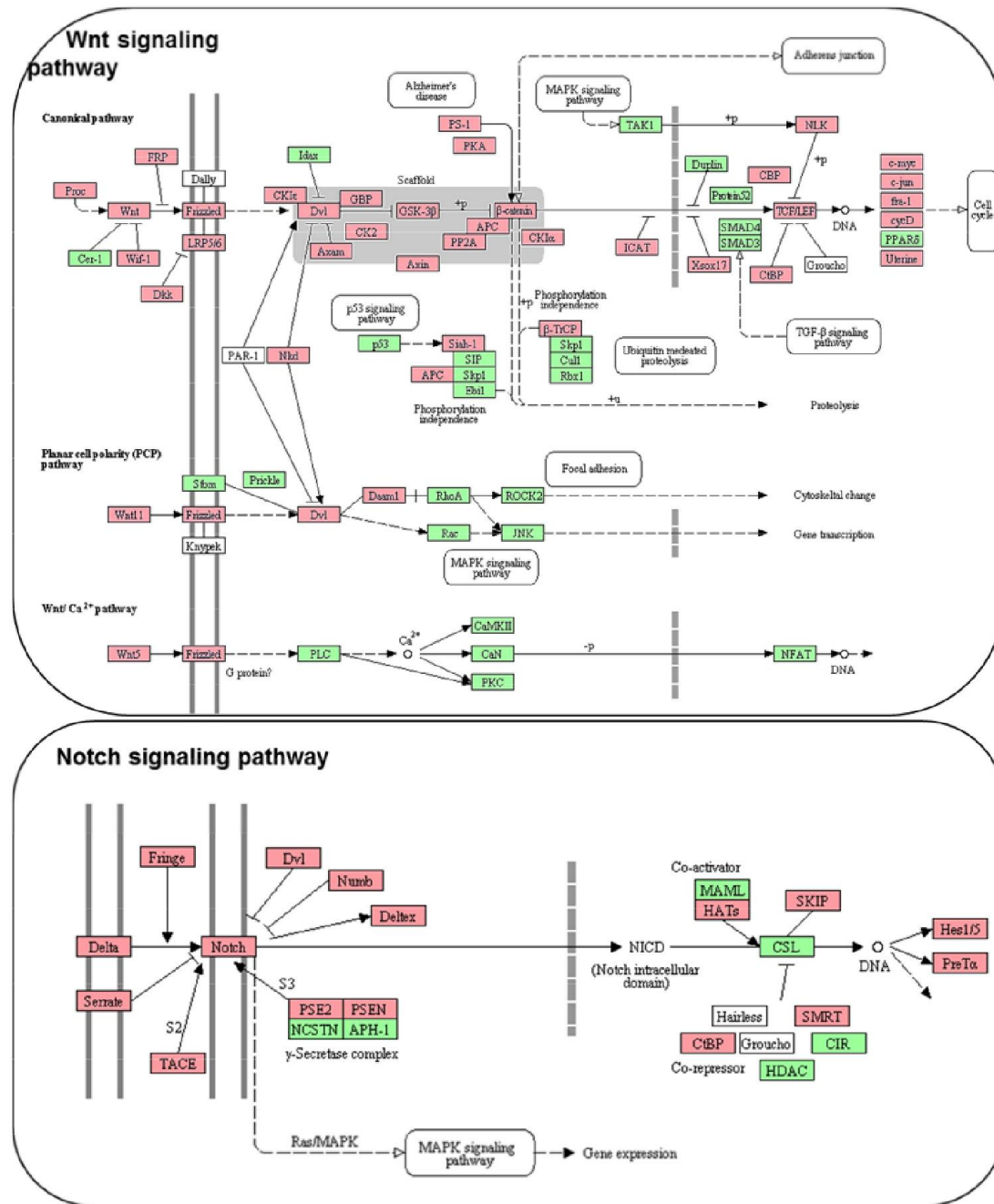


Figure S9: Wnt and Notch signaling pathways in the stomach after vagotomy in INS-GAS mice. Wnt and Notch signaling KEGG pathways in the anterior oxyntic mucosa after anterior unilateral vagotomy compared with the posterior side at 6 months postoperatively. Down-regulated genes ($p < 0.05$) are indicated by pink; unchanged genes are green.

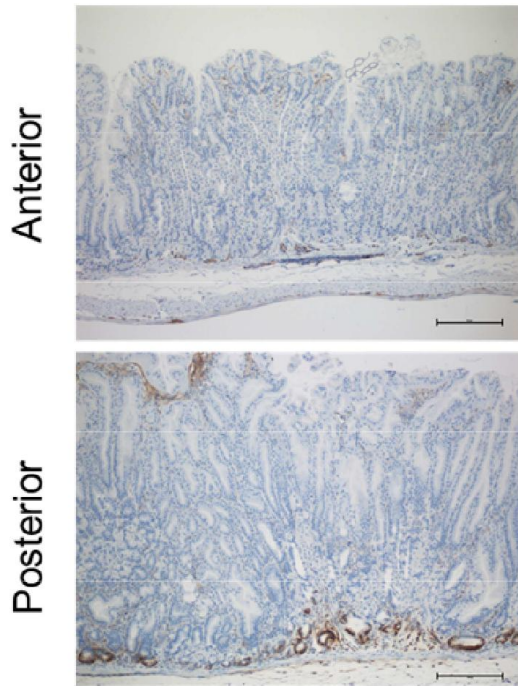


Figure S10: Immunostaining of CD44 after vagotomy in INS-GAS mice. Representative microphotographs of CD44+ cells in the oxyntic mucosa of the anterior and the posterior regions of the same stomach in a mouse subjected to unilateral anterior vagotomy (UVT).

Scale bars = 25 μ m.

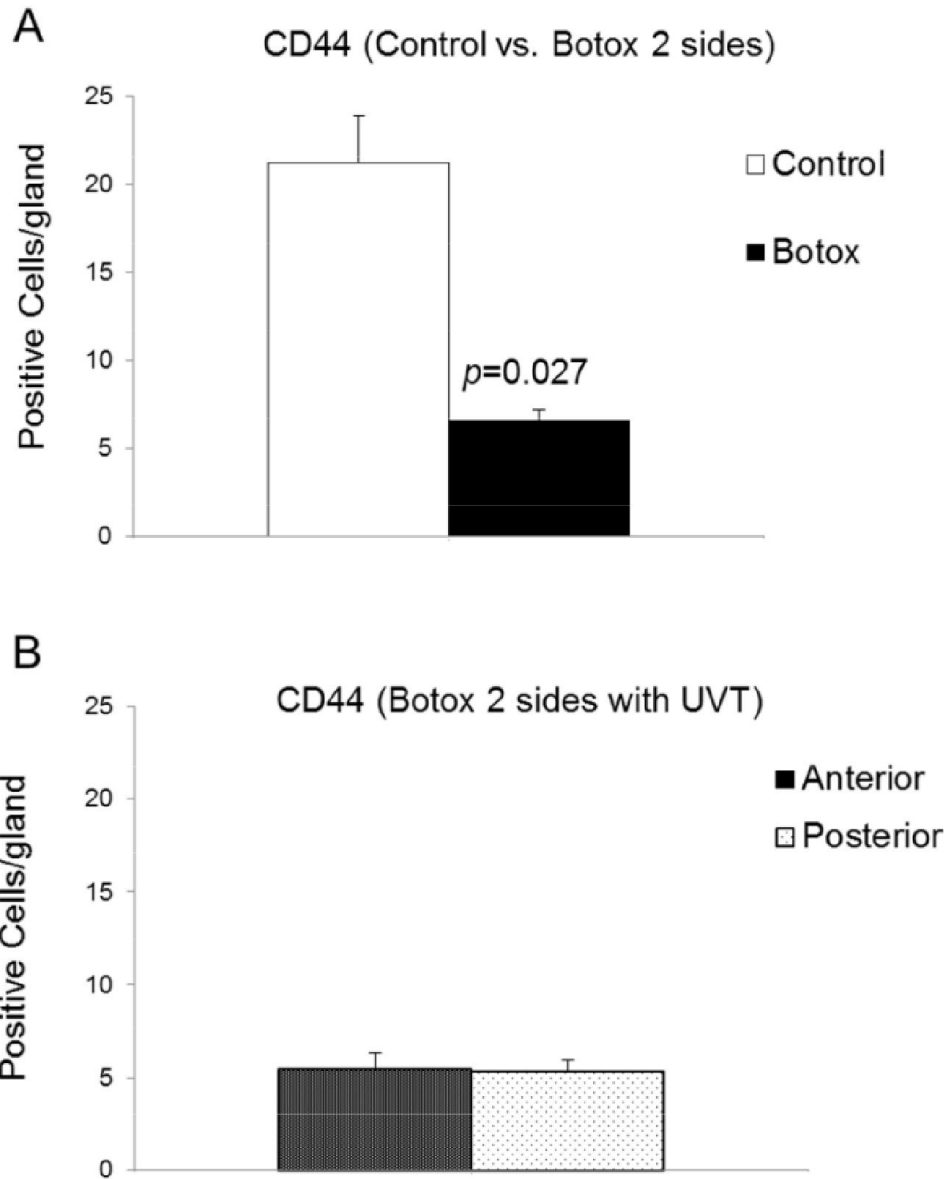


Figure S11: Numbers of CD44-immunoreactive cells after Botox treatment ± vagotomy in INS-GAS mice. CD44-immunoreactive cells in mice subjected to saline (control) or Botox injection into anterior and posterior sides of the stomach (A) and Botox injection into anterior and posterior sides plus anterior UVT (B). Means ± SEM. Student's *t* test was used to compare control ($N = 6$) and Botox ($N = 7$).

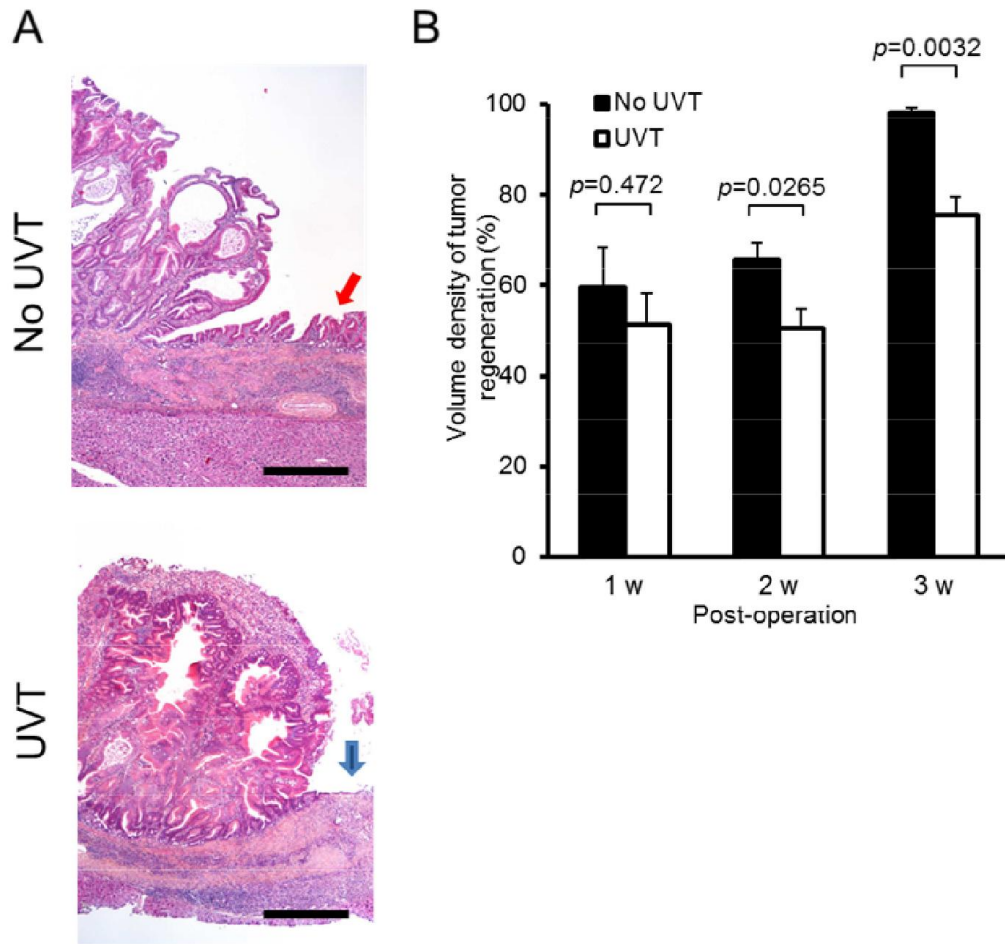


Figure S12: Tumor regeneration in the stomach after vagotomy in INS-GAS mice. (A) Microphotographs showing histopathological appearances of tumor regeneration at 3 weeks after acetic acid-induced necrotic ulcer. Note regeneration (indicated by red arrow) without unilateral vagotomy (No UVT) and no regeneration (blue arrow) after UVT. Scale bars: 50 μm . (B) Volume density of tumor regeneration 1, 2, and 3 weeks after application of acetic acid in mice with or without UVT. Means \pm SEM. Student's *t* test was used to compare no UVT and UVT ($N = 6$, except $N = 8$ or 5 , respectively, at 3 weeks).

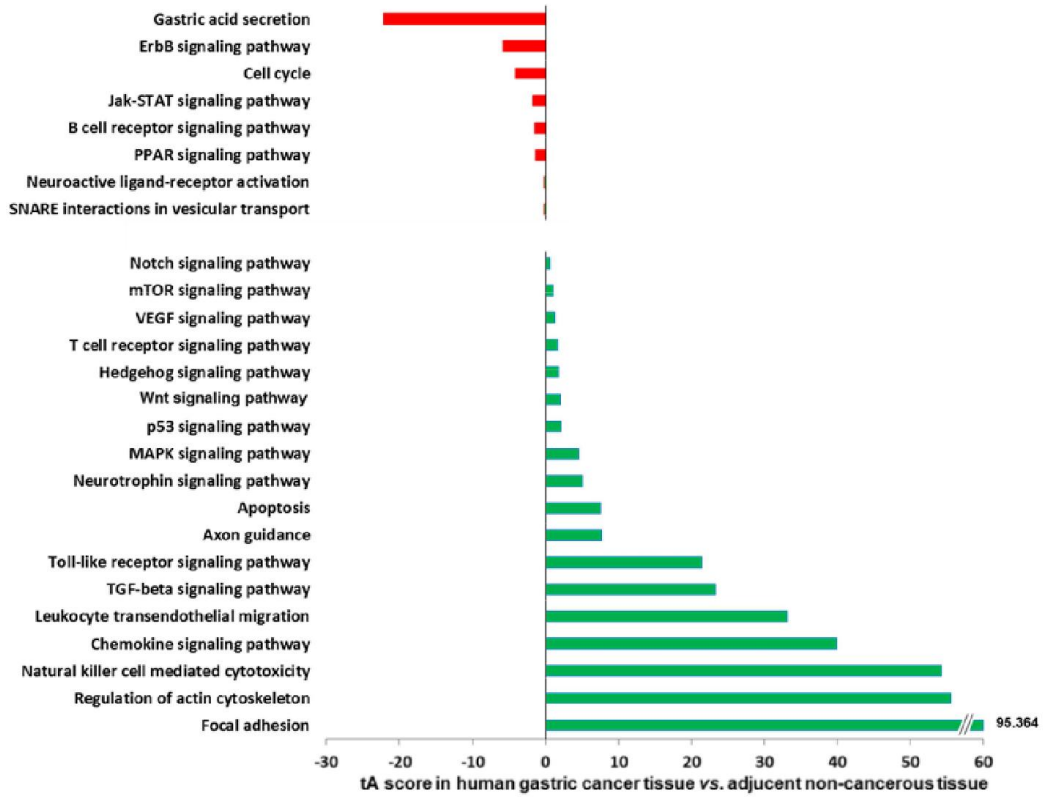
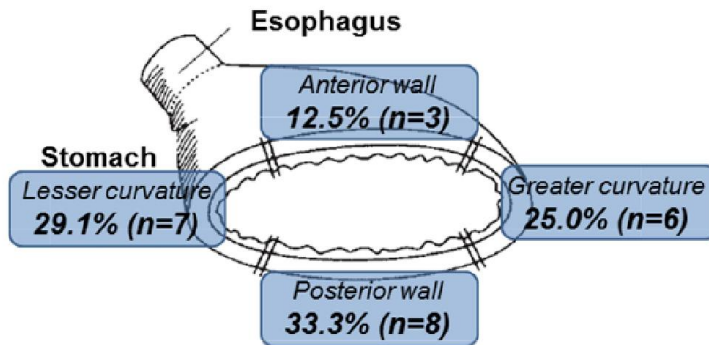


Figure S14: Altered signaling pathways in human gastric cancer tissue compared with adjacent noncancerous tissue. tA score>0: activation (indicated by green); tA score<0: inhibition (red)

A Non-vagotomized patients (n=24)



B Vagotomized patients (n=13)

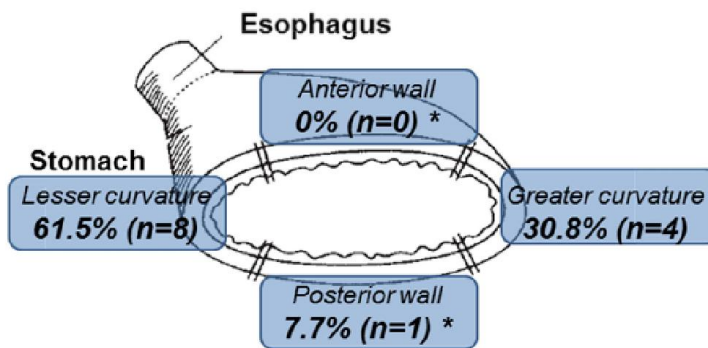


Fig. S15. Gastric stump cancer after distal gastrectomy with or without vagotomy. (A) Tumors in both anterior and posterior walls in 24 patients without vagotomy. (B) No tumors in anterior and one tumor in a posterior wall among 13 patients who underwent vagotomy. $p = 0.01898$ or $p = 0.02718$ for anterior or posterior wall of vagotomized patients compared with non-vagotomized patients (Fisher test).

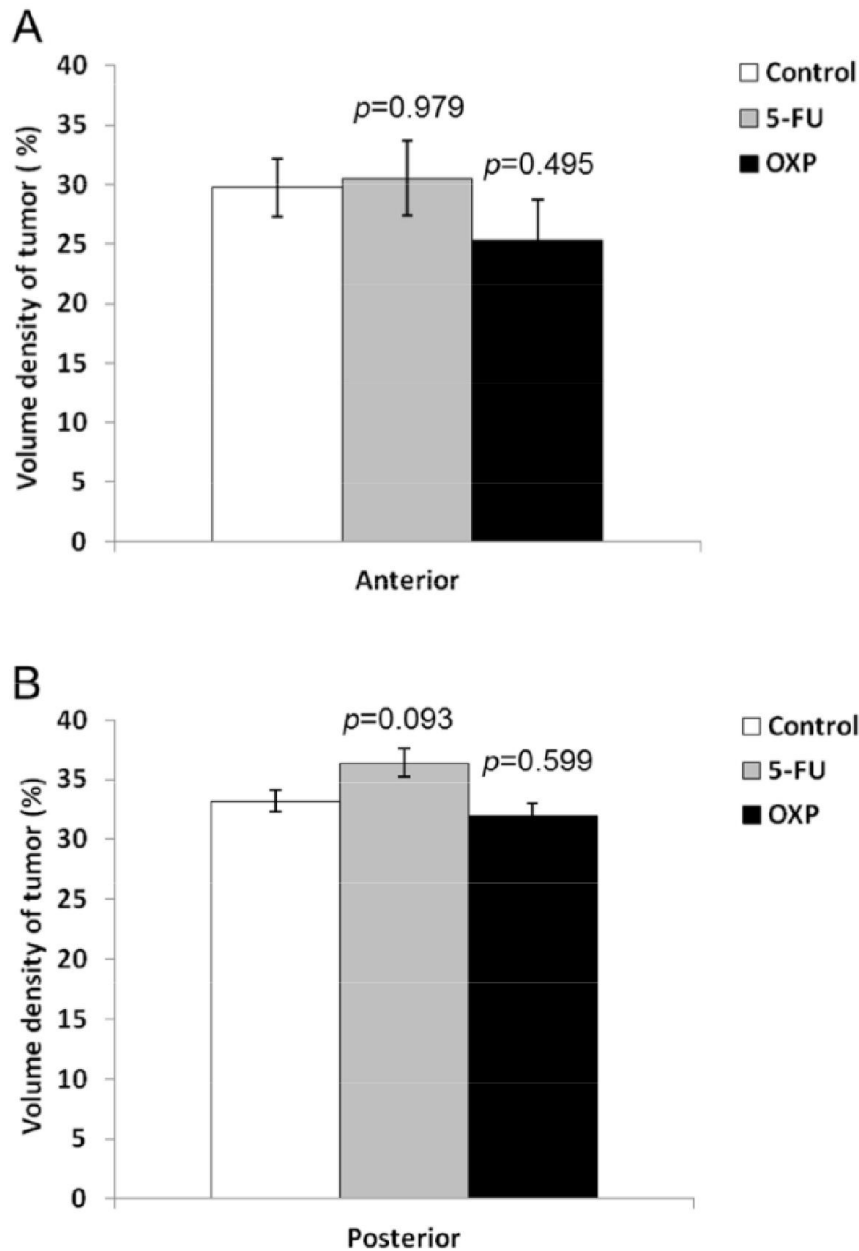


Fig. S16. Effect of 5-FU and oxaliplatin on INS-GAS mice. Tumor size in the anterior (A) or posterior (B) sides of stomachs in mice treated with saline (Control, $N = 10$), 5-FU ($N = 10$), or oxaliplatin (OXP, $N = 13$). Means \pm SEM. P values were calculated by Dunnett's test.

Table S1. Animal experimental groups.

	Mouse (N)	Group (N)	Age* at operation (months)	Age* at examination (months)
1	INS-GAS (107)	Sham (27)	6	12
		PP (25)	6	12
		UVT (30)	6	12
		VTPP (25)	6	12
2	MNU (FVB)(20)	MNU+ PP(11)		13
		MNU+VTPP (9)	3.5	13
3	<i>H.p.</i> -infection (24)	Sham (12)	12	18
		UVT (12)	12	18
4	INS-GAS (16)	UB (16)	6	12
5	INS-GAS (64)	No surgery (21)		18
		UVT (17)	8	18
		UVT (14)	10	18
		UVT (12)	12	18
6	INS-GAS (26)	Vehicle (6)	12	14
		UB (6)	12	14
		BB (7)	12	14
		BB+UVT (7)	12	14
7	INS-GAS (133)	No treatment (12)	12-14	14-16
		Saline (10)	12-14	14-16
		5-FU (10)	12-14	14-16
		OXF (13)	12-14	14-16
		UB+Saline (10)	12-14	14-16
		UB+5-FU (10)	12-14	14-16
		UB+OXF (13)	12-14	14-16
		Sham+5-FU+OXF (15)	12-14	14-16
		UB+5-FU+OXF (24)	12-14	14-16

	UVT+5-FU+OXP (16)	12-14	14-16
8 INS-GAS (16)			
	UVT (5)	6	8
	UVT (5)	6	10
	UVT (6)	6	12
9 INS-GAS (64)			
	Saline (19)	12-14	14-16
	5-FU+OXP (12)	12-14	14-16
	Darifenacin (15)	12-14	14-16
	5-FU+OXP+darifenacin (8)	12-14	14-16
10 INS-GAS (12)	INS-GAS - No treatment (6)	6	12
FVB (20)	INS-GAS - UVT (6)	6	12
	WT- No treatment (10)	6	12
	WT- UVT (10)	6	12
11 MNU (12)			
	PP (6)	6	10
	VTPP (6)	6	10
12 M3KO (7)	M3KO+MNU (7)		11
C57BL/6 (13)	WT+MNU (13)		11
13 INS-GAS (37)			
	Regeneration** 1 week (6)	12-18	12-18+1week
	Regeneration 1 week after UVT (6)	12-18	12-18+1week
	Regeneration 2 weeks (6)	12-18	12-18+2weeks
	Regeneration 2 weeks after UVT (6)	12-18	12-18+2weeks
	Regeneration 3 weeks (8)	12-18	12-18+3weeks
	Regeneration 3 weeks after UVT (5)	12-18	12-18+3weeks
14 Lgr5-GFP (10)			
	MNU + PP (5)	4,75	6,25
	MNU+ VTPP (5)	4,75	6,25

PP: Pyloroplasty, UVT: Unilateral vagotomy, VTPP: Bilateral vagotomy+pyloroplasty

UB: Unilateral Botox injection, BB: Bilateral Botox injection, OXP: Oxaliplatin

*Preneoplasia at 6 months and neoplasia at 12 months of age in INS-GAS mouse. **Tumor regeneration was induced by topical application of acetic acid.

Table S2. Cohorts of gastric cancer patients.

	1st cohort	2nd cohort	3rd cohort
Country	Norway	Japan	Japan
Purpose	Gene expression profiling	Innervation and tumorigenesis	Stump cancer after vagotomy
Study period	2005-2010	2001-2008	1962-1998
Patient			
Number (male:female)	17 (14:3)	120 (78:42)	37 (31:6)
Age (y.o.)	49-86	31-92	69-90
Pathological stage	I-IV	II-IV	I-II
<i>H.pylori</i> status	10/17 positive	n.d.	n.d.

Table S3. List of qRT-PCR primers used in this study.

Gene	Forward (5'->3')	Reverse (5'->3')
<i>Lgr5</i>	TCCAACCTCAGCGTCTTC	TGGGAATGTGTGTCAAAG
<i>Cd44</i>	CACATATTGCTTCAATGCCTCAG	CCATCACGGTTGACAATAGTTATG
<i>Axin2</i>	ACTGACCGACGATTCCATGT	TGCATCTCTCTCTGGAGCTG
<i>Myc</i>	AGAGCTCCTCGAGCTGTTTG	TGAAGTTCACGTTGAGGGG
<i>Cyclin D1</i>	TCCTCTCCAAAATGCCAGAG	GGGTGGGTTGGAAATGAAC
<i>Sox9</i>	AGGAAGCTGGCAGACCAGTA	TCCACGAAGGGTCTCTTCTC
<i>Chrm1</i>	CAGAAGTGGTGATCAAGATGCCTAT	GAGCTTTTGGGAGGCTGCTT
<i>Chrm2</i>	TGGAGCACACAAGATCCAGAAT	CCCCTGAACGCAGTTTTCA
<i>Chrm3</i>	CCAGTTGGTGTGTTCTTCCTT	AGGAAGAGCTGATGTTGGGA
<i>Chrm4</i>	GTGACTGCCATCGAGATCGTAC	CAAAC TTTCGGGCCACATTG
<i>Chrm5</i>	GGCCCAGAGAGAACGGAAC	TTCCCGTTGTTGAGGTGCTT
<i>Gapdh</i>	TCATTGTCATACCAGGAAATGAG	AGAAACCTGCCAAGTATGATGAC